AFRL-AFOSR-UK-TR-2022-0003

Goal of 10 GHz Mode locked mid-IR Microchip Waveguide Lasers

Kar, Ajoy
HERIOT-WATT UNIVERSITY
RICCARTON
EDINBURGH, MIDLOTHIAN, EH14 4AS
GBR

11/04/2021
Final Technical Report

Air Force Research Laboratory
Air Force Office of Scientific Research
European Office of Aerospace Research and Development
Unit 4515 Box 14, APO AE 09421

REPORT DOCUMENTATION PAGE

Form Approved
OMB No. 0704-0188

1. REPORT DATE *(DD-MM-YYYY)*	**2. REPORT TYPE**	**3. DATES COVERED** *(From - To)*
04-11-2021	Final	15 Jun 2018 - 14 Jun 2021

4. TITLE AND SUBTITLE
Goal of 10 GHz Mode locked mid-IR Microchip Waveguide Lasers

5a. CONTRACT NUMBER

5b. GRANT NUMBER
FA9550-18-1-0202

5c. PROGRAM ELEMENT NUMBER
61102F

6. AUTHOR(S)
Ajoy Kar

5d. PROJECT NUMBER

5e. TASK NUMBER

5f. WORK UNIT NUMBER

7. PERFORMING ORGANIZATION NAME(S) AND ADDRESS(ES)
HERIOT-WATT UNIVERSITY
RICCARTON
EDINBURGH, MIDLOTHIAN EH14 4AS
GBR

8. PERFORMING ORGANIZATION REPORT NUMBER

9. SPONSORING/MONITORING AGENCY NAME(S) AND ADDRESS(ES)
EOARD
UNIT 4515
APO AE 09421-4515

10. SPONSOR/MONITOR'S ACRONYM(S)
AFRL/AFOSR IOE

11. SPONSOR/MONITOR'S REPORT NUMBER(S)
AFRL-AFOSR-UK-TR-2022-0003

12. DISTRIBUTION/AVAILABILITY STATEMENT
A Distribution Unlimited: PB Public Release

13. SUPPLEMENTARY NOTES

14. ABSTRACT

25 June 2021: Site Visit of Heriott-Watt University, Scotland, United Kingdom. Dr. Nathaniel Lockwood and Dr. Attila Szep, AFOSR/IOE, conducted a visit of Heriott-Watt University led by Dr. Richard Carter and Dr. Richard McCracken. Prof Ajoy Karr, Heriott-Watt University, Unite Kingdom in collaboration with researchers at Milano Polytechnic, Italy developed a room temperature Kerr-lensing mode (KLM) locked Chromium and Iron doped Zinc Selenide (Cr:ZnSe) II-VI material laser, which is centered at 2.4 micron wavelengths. The KLM allows self-compression of the pumping diode laser, creating extremely short temporal (< 10-13 seconds high pulse rate, intense laser pulses. It essentially compresses a small amount of laser energy into a very short amount of time to generate militarily useful non-linear effects in the target at low overall low system power. This wavelength is important because it represents a higher power transmission window than standard 1 to 1.6 micron wavelength lasers operate in, making the KLM laser highly useful for Infrared Counter Measures (IRCM). The ZnSe was doped using Hot Isostatic Pressing (HIP) treatment also developed and optimized under a previous EOARD Grant and transitioned to AFRL/RYD. The laser operates with a pulse repetition frequency (PRF) of 182 MHz demonstrating at an average output power of 140 milli-Watts. The KLM laser output power was simply limited due to the lack of funding to create a thermal management system to enable increased power. The most valuable outcome of the research however was that he achieved ultra-short pulsed laser (USPL) durations, down to 37 femto-seconds (fs), by exploiting intra-cavity chirped mirrors for dispersion control. To achieve these short pulse durations, a world-record for ZnSe, typically requires a very large series of stretching and compressing diffraction gratings and optics, however the Cr:ZnSe KLM laser achieved this in a space of < 30 cm x 30 cm x 8 cm with an X-fold laser geometry. These KLM USPL pulses are significant to the USAF because they can achieve non-linear disruptive effects within the target at low laser energy levels, thus significantly reducing the size and power requirements for the military platform. ZnSe was introduced as an active gain media in the mid-90s and has become arguably the most favored laser source in the mid-IR and long wave-IR spectral region. ZnSe directly stimulated emission at wavelengths spanning 1.8-6 Î¼m in the form of a compact solid-state laser source. Prof Karr has also proved room temperature Fe:ZnSe and Fe:ZnS are extremely useful for a tuneable KLM laser emission in the very valuable application of IRCM and optimal to power transmission 3.4-5.2 Î¼m wavelength range at nano-second pulse widths. Emission in this spectral region until recently tended to be dominated by rather bulky and complex, gas lasers as well as OPO set-ups based on down conversion of a near IR solid-state laser source.

15. SUBJECT TERMS

16. SECURITY CLASSIFICATION OF:			**17. LIMITATION OF ABSTRACT**	**18. NUMBER OF PAGES**	**19a. NAME OF RESPONSIBLE PERSON**
a. REPORT	**b. ABSTRACT**	**c. THIS PAGE**			NATHANIEL LOCKWOOD
U	U	U	SAR	65	**19b. TELEPHONE NUMBER** *(Include area code)* 314-235-6005

Goal of 10 GHz Mode Locked Mid-IR Microchip Waveguide

Progress Review
15 June 2018 to 14 June 2021
Award Number: FA9550-18-1-0202

A K Kar
Institute of Photonics and Quantum Sciences Heriot-Watt University
Edinburgh EH14 4AS, Scotland
a.k.kar@hw.ac.uk

Contents

Introduction

This report details the work cared out at Heriot-Watt University over the last three years on the project titled "Goal of 10 GHz Mode Locked Mid-IR Microchip Waveguide "fabricated by ultrafast laser inscription (grant award number FA9550-18-1-0202). This research was done in very close collaboration with the Novel Laser Technologies group at Sensors Directorate AFRL/RYDH at WPAFB in the USA. In this report we will detail our development of Cr^{+}:ZnSe mode locked laser in which we have demonstrated Kerr-Lens Mode locked (KLM) lasers in both bulk and Hot Isostatic Pressed wavelength tuneable laser operation. The most significant results are the report of sub-50fs pulses from both bulk and HIP treated Cr^{+}:ZnSe lasers. A detailed theoretical studies have also been undertaken in modelling the self-focussing and the coupling of various waveguides in the Cr^{+}:ZnSe waveguides. This is a stepping stone for the development of the future holistic KLM Cr^{+}:ZnSe lasers

The work in this report has been done during the past year as part of a long term collaboration between Heriot Watt University (HWU) and the Air Force Research Laboratory (AFRL). The main participants in this collaboration this year have been at HWU; research group leader A. K. Kar and his group members F. Thorburn and A. Lancaster and at AFRL; G. Cook, S. A. McDaniel and C Liebig. This work has been able to progress for another year due to continued funding from EOARD. All of the work was made possible my continued funding form EOARD. KLM mode locking was undertaken in the Politecnico di Milano in collaboration with Dr Gianluca Galzerno.

We are also reporting on the ongoing experiment the direct comparison of the performance off KLM of both bulk and HIP Cr:ZnSe. In addition a comparative study are also in progress for the most suitable pumping source for Cr:ZnSe.

Cr^{+}:ZnSe Mode locked Laser

Introduction

In recent years, there has been a significant growth in demand for sources in the mid-infrared spectral region which spans 2-5 μm. The requirement for laser sources in this spectral region is driven by the vast amount of applications. This is because this wavelength range contains a number of atmospheric transmission windows. A number

of characteristic molecule absorption lines lie in this mid-IR spectral band, hence there are a great many opportunities for environmental monitoring and sensing using these sources [1]. Other examples of mid-IR laser source applications include medical diagnostics and treatment [2], military and defence [3], and high-precision material processing [4]. The requirements of a particular source, that is the wavelength, power capabilities, size, running and maintenance costs, are very much dependent on the specific application. Previously, there had been an absence of sources which emit in this region due to a lack of semiconductor materials with suitable bandgap energies compared to the IR and visible spectral regions. Subsequently, there has been significant effort and funding invested to discover and develop new sources emitting here which can satisfy the specific requirements for the vast array of applications. For many of these applications pulsed sources are preferred. In particular, sources with ultrafast pulses and high pulse repetition frequencies (PRFs) are required for applications such as high speed optical communication and optical frequency combs for precision metrology [5-7]. The high PRFs are needed for these types of applications to facilitate the high level of resolution and precision necessary. The motivation behind this work is to explore new mid-IR laser source systems which are compact, robust and furthermore, have the potential ability for the generation of ultrafast pulses with GHz pulse repetition frequencies (PRFs). Hence, they would overcome many of the challenges associated with the commonly used sources at present.

During the past ~ 20 years transition metal doped II-VI semiconductors (TM:II-VIs) have emerged as a promising solution to the lack of emission sources in the mid-IR. Examples of such II-VI semiconductor hosts are ZnS, ZnSe, CdSe and CdMnTe, the most common dopants for mid-IR emission are Cr and Fe. Laser wavelengths throughout the mid-IR from ~ 1.8 μm to ~ 6 μm have been demonstrated with continuous tuneablity achieving CW output powers ranging from 10s of mW to > 100 W. One particular material which has been researched extensively is Cr^{2+} doped Zinc Selenide (Cr:ZnSe). Cr:ZnSe has been shown to have continuously tuneable lasing capability spanning over 1300 nm from 1973-3349 nm [8] and the maximum output power demonstrated to date in this material is 140 W with an optical efficiency of 62% [9]. The broad spectral emission capability of Cr:ZnSe means it is particularly suitable for ultrafast pulse generation in the mode locked regime. This report presents the results of a room temperature mode locked Cr:ZnSe bulk laser in which this gain

medium has been treated with Hot Isostatic Pressing (HIP) treatment. The laser operates with a PRF of 182 MHz and average output power of 140 mW is demonstrated. Pulse durations down to 37 fs are achieved by exploiting intracavity chirped mirrors for dispersion control. This result represents the shortest pulse duration demonstrated to date in Cr:ZnSe. The reasons that the HIP process has facilitated this record result are discussed. We also presents from a preliminary investigation in which ultrafast mid-IR pulses are amplified in a Cr:ZnSe waveguide which was fabricated by Ultrafast Laser Inscription (ULI). The waveguide amplifier exhibits an internal gain factor of 5.375.

Ultrafast Hot Isostatic Pressed Cr:ZnSe Laser at ~ 2.4 µm

TM:II-VIs were introduced as active gain media in the mid-90s [10], since then they have become the arguably the most favoured emission sources in not only the mid-IR, but also at longer wavelengths into the far-IR spectral region. This is because they provide a means to directly stimulate emission at wavelengths spanning 1.8-6 µm in the form of a compact solid-state laser source. Previously, emission in this spectral region tended to be dominated by rather bulky and complex, gas lasers as well as OPO setups based on down conversion of a near IR solid-state laser source. TM:II-VI lasers largely replaced these generation methods [11]. Despite laser diodes and QCLs also finding some success in this market [12, 13], they tend to be limited to small emission ranges compared to very broad bandwidths which are typical of TM:II-VI lasers.

II-VI semiconductors are ideal as a choice for a host material due to their low phonon energy, wide band-gap, broad transmission range and a crystal structure which is readily acceptant of TM dopant ions [14]. The TMs are elements which lie on the periodic table between Scandium and Zinc. They are defined as having a partially filled d orbital. When doped into a crystal, the resultant spectral emissions are extremely sensitive to the local field of that host crystal. This sensitivity is a consequence of electron-phonon interactions. These interactions can occur because the outer 3d-electrons are unshielded permitting them to couple strongly to surrounding phonons. This leads to 3d-3d absorption and emission bands which are the transitions laser action is based on. The strong electron-phonon coupling also leads to the TM ions experiencing vibronic broadening of the energy transitions; the resultant broad emission bandwidths, often spanning 10s to 100s of nm, are characteristic of TM

doped laser sources [15].The most common example of such a broad emission profile from a TM doped solid-state laser is Ti:Sapphire which has emission spanning ~ 680-1100 nm [16].

When TMs are doped into the tetrahedral crystal field of an II-VI semiconductor such as ZnSe, the ^5D ground state of the dopant ion is split into a triplet $^5T_2$ level and a doublet ^5E level by crystal-field splitting. It is between these two vibronically broadened levels in which absorption/emission transitions are allowed leading to laser action, whereas transitions to higher levels are spin forbidden resulting in high gain with zero ESA [17]. The broad emission profiles are not only due to the vibronic broadening, there is also a contribution from the Jahn-Teller effect [14]. This causes further splitting of the two electronic energy levels originating from a distortion of the crystal. The full implications of the Jahn-Teller effect on TM:II-VI lasers are not fully agreed on within this field of research, but it is widely accepted that it does contribute to the broadening of energy transitions. More information on the Jahn-Teller effect on TM:II-VI media can be found in [18-20]. The combined effect of the vibronic broadening and Jahn-Teller effects discussed result in an approximate four level laser system [21].

The most well-known and commonly used combinations for laser emission in the mid-IR are ZnSe and ZnS doped with Fe^{2+} and Cr^{2+}. For simplicity these combinations are here on referred to as Cr:ZnSe and Cr:ZnS, as well as for Fe. Although Fe:ZnSe and Fe:ZnS are extremely useful for tuneable emission in the 3.4-5.2 μm range, to exploit this potential as a CW source it is necessary to cool the crystal down to ~ 150 K, otherwise they can operate as pulsed ns sources at room temperature [22]. Cooling to such temperatures is disadvantageous as it adds considerable cost whilst also complicating the system. On the other hand Cr:ZnSe and Cr:ZnS have demonstrated excellent room temperature performance from CW to the fs regime. Furthermore, they have shown impressive tuneable performance spanning the range of 1973-3349 nm and 1962-3195 nm respectively [8]. The absorption and emission cross sections of these materials are displayed in Figure 1.

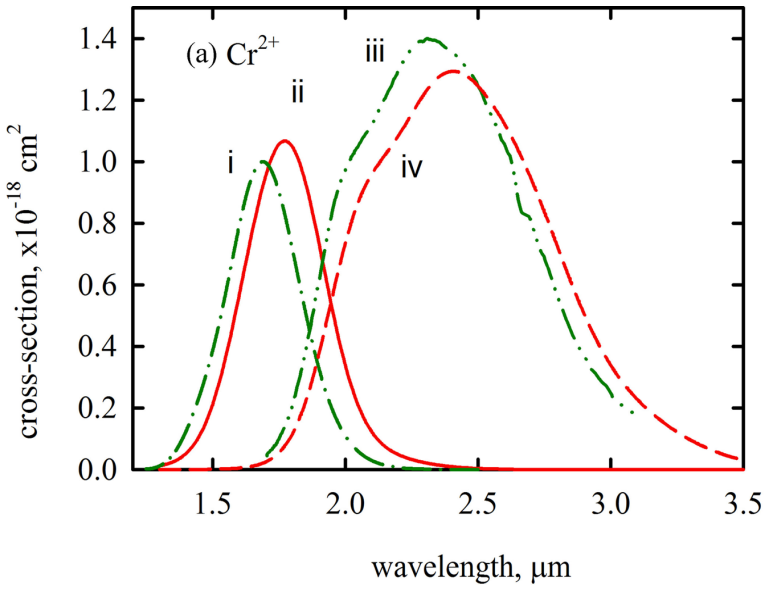

Figure 1. Curves i) and iii) represent the absorption and emission cross sections respectively in Cr:ZnS. Similarly ii) and iv) represent those in Cr:ZnSe. Diagram has been reproduced from [21].

For emission in the mid-IR these materials can be pumped with sources ranging ~ 1.4 – 2.1 μm. Therefore, they are most commonly pumped with commercially available ~ 1.9 μm and ~ 1.5 μm Tm and Er fibre lasers.

With regards to emission specifically in the mode locked regime, should the entire bandwidth of Cr:ZnSe be used to emit mode locked pulses, there is the potential for the generation of only 6 fs $sech^2$ profile pulses. To date, no one has reported modelocking of the full bandwidth of either crystal but various SA's and mode locking techniques have been successfully implemented with these materials to result in ultrafast pulses. A summary of some of the most notable mode locking results obtained in Cr:ZnSe with different mode locking and group delay dispersion (GDD) compensation methods is presented in Table 1.

Saturable Absorber Type	Pulse Duration	Pulse Repetition Frequency	GDD Compensation Method	Laser Average Output Power	Reference	Year reported
Cr:ZnSe						
AOM	4.4 ps	81 MHz	none	82 mW	[23]	2000
SESAM	11 ps	100 MHz	none	400 mW	[24]	2005
SESAM	100 fs	200 MHz	Sapphire window	75 mW	[25]	2006
SESAM	80 fs	180 MHz	Chirped mirrors	80 mW	[26]	2007
Kerr-lens	100 fs	100 MHz	YAG window	300 mW	[27]	2009
Graphene based SA	226 fs	77 MHz	CaF prism pair	80 mW	[28]	2013
Combination of Graphene and Kerr-lens	116 fs	99 MHz	CaF prism pair	66 mW	[29]	2014
Kerr-lens	43 fs	83 MHz	Dispersive mirrors**	250 mW	[30]	2014
Kerr-lens	47 fs 60 fs	150 MHz 300MHz	Chirped mirrors	300 mW 250 mW	[31]	2017
Kerr-lens	45 fs	65 MHz	Dispersive mirror and sapphire plate	500 mW	[32]	2019

It is evident from this table that Kerr-lens mode locking (KLM) coupled with optimum GDD compensation has led to generation of the shortest pulses. Until this work, the shortest pulse width emitted from Cr:ZnSe were in the range of 43-47 fs as reported in [30-32]. With regards to repetition rate, no GHz fs sources have been reported in Cr:ZnSe, the highest PRFs demonstrated are ~ 300 MHz and the pulse width tends to increase at higher PRFs as demonstrated by Yang et al. [31].

As ULI has facilitated the development of robust, efficient and extremely compact Cr:ZnSe laser sources which effectively eliminate thermal lensing effects, these may provide an ideal method of achieving a GHz mode locked source. Experiments exploring the use of a commercial SESAM in combination with a single mode depressed cladding Cr:ZnSe waveguide laser have been performed by a previous member of the NLO group in [33] and also partly presented by colleagues from the AFRL in [34]. The authors claimed at this time that the waveguide laser emitted ~ 1.5 ps pulses at a PRF of 960 MHz and ~ 0.6 ps pulses at the reduced PRF of 308 MHz.

The autocorrelation trace and corresponding wavelength spectrum obtained for the two different PRFs are shown in Figures 2 and 3.

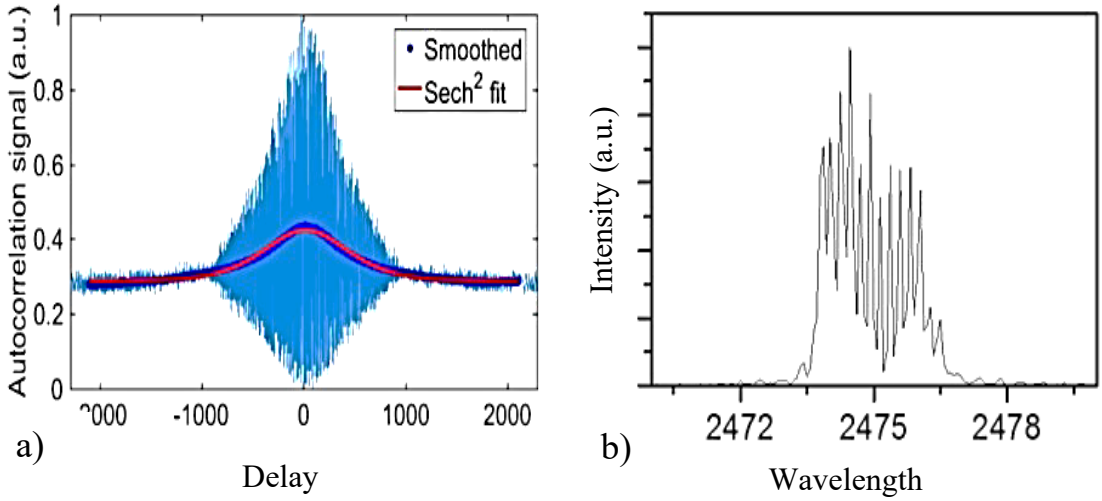

Figure 2. a) Autcorrelation trace and b) Wavelength spectrum obtained from SESAM modelocked Cr:ZnSe ULI waveguide laser at 308 MHz. a) measures a pulse duration of 0.6 ps. Graphs have been reproduced from [34].

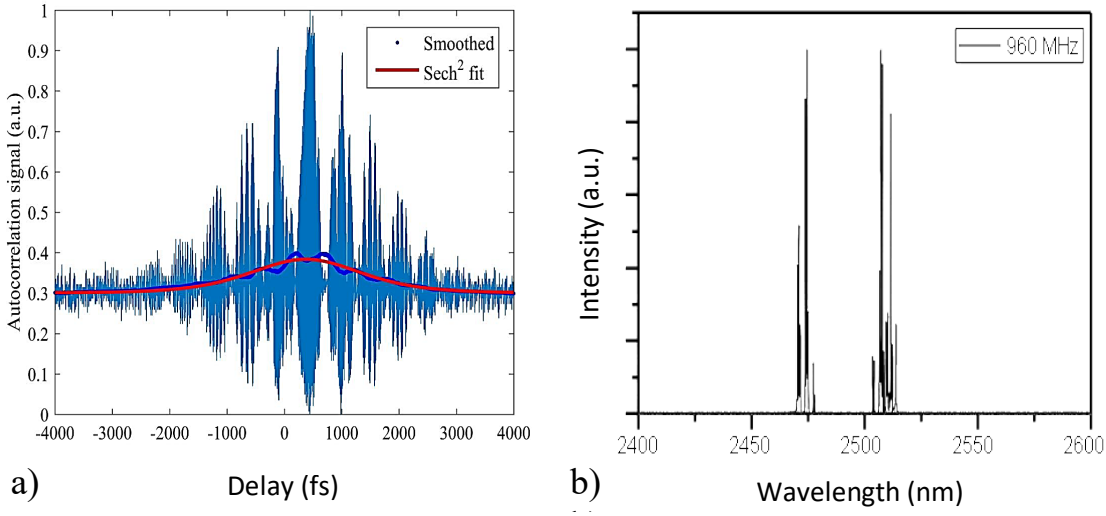

Figure 3. a) Autcorrelation trace and b) Wavelength spectrum obtained from SESAM mode locked Cr:ZnSe ULI waveguide laser at 960 MHz. a) measures a pulse duration of 1.5 ps. Graphs have been reproduced from [33].

It can be clearly seen from Figures 2 and 3 that in both cases the autocorrelations traces presented do not exhibit the 8:1 peak to wing ratio characteristic of a CW mode locked laser. The trace in Figure 3a) also exhibits an interference effect not common to standard autocorrelation traces. This explained by the suggestion of interference of

the two different emission bands which appear in the corresponding wavelength spectrum in Figure 3(b). Although these results are indicative of mode beating occurring in the cavity, further investigations are required to clarify if the laser is indeed operating in the CW mode locked regime and why the pulse measurements do not have the correct ratio.

Simultaneous to this work, our colleagues at the AFRL also reported significant results concerning the use of Hot Isostatic Pressing Treatment on TM:II-VI materials [35]. This paper presents results of utilising HIP for both the actual diffusion of the TMs into the host and as a post dopant treatment to an already diffusion doped sample. In both cases the result is that the laser spectral linewidth in a bulk resonator is reduced from spanning typically 10s of nm to sub-nm levels. Consequently, efforts were aimed at inscribing ULI waveguides in HIP treated Cr:ZnSe and utilising a SESAM to compare results to the untreated material with the aim of developing a high PRF source. However, it was found that the waveguide inscription parameters for the untreated material resulted in high loss waveguides in HIP treated material. Therefore investigations into identifying the optimum parameters are ongoing. As a consequence of this, and also the recent results exploiting KLM in Cr:ZnSe shown in Table 1, we postulated that investigating the use of bulk HIP treated Cr:ZnSe with KLM would be useful to assess its performance for the generation of fs pulses compared to untreated bulk Cr:ZnSe. Hence this could enhance understanding of the full effect of the HIP treatment. Thus we will present results of a HIP treated Cr:ZnSe bulk laser in the CW and KLM regimes respectively.

HIP is a material treatment process in which both high temperature and pressure, typically > 100 MPa and 500^{o}C respectively, are applied concurrently to a material in a container designed to withstand such conditions [36]. In general, HIP treatment has been used to improve the mechanical properties of metal based materials for applications such as upgrading castings and consolidating powders [35, 36]. However, it has also found use in some optical applications for the manufacture and preparation of ceramic laser crystals [37]. Specifically for the case of materials used in TM:II-VI semiconductors, HIP treatment has previously been shown to grow the grain sizes in undoped ZnSe [38] and latterly it was shown that it can also remove defects in Cr:ZnSe [39]. Most recently, Stites et al. [35] published a report in which they describe the

process of utilising HIP treatment to force-diffuse Cr ions which were sputtered on to a ZnSe host surface [35]. The samples were held in argon gas at 1050°C at 30,000 PSI for two hours. This ultimately results in extremely narrow, < 140 pm, linewidth laser output from a standard z-fold bulk laser cavity. They also demonstrate that the narrow linewidth occurs when a commercially bought sample of Cr:ZnSe is HIP treated, proposing that the reason for the spectral narrowing is that the HIP treatment converts inhomogeneously broadened material to homogeneously broadened material. The treatment causes this conversion by acting to remove crystalline defect centres and growing the grain size thus reducing the number of grain boundaries in the crystal. These are believed to be the sources of strong inhomogeneous broadening exhibited in commercially available untreated polycrystalline Cr:ZnSe [35]. The effect has also been demonstrated in a Fe:ZnSe bulk laser [40].

The mode locking investigation which will be presented has been carried out in collaboration with colleagues based in Politecnico di Milano. Prior to these experiments, a preliminary CW characterisation of a HIP treated Cr:ZnSe crystal was carried out in our labs at HWU where we have a 1.9 μm Thulium doped fibre pump laser. The results of this initial CW investigation will be presented first.

HIP Treated Cr:ZnSe Laser pumped at 1.9 μm

The Cr:ZnSe sample utilised in this experiment had dimensions 3 × 6 × 7 mm and a dopant concentration of 6.05×10^{18} cm^{-3}. The sample was fabricated by IPG photonics and subsequently treated with HIP. The HIP process is as follows: the sample was sealed within a chamber designed to withstand high temperatures and pressure, subsequently the temperature and pressure were raised over the course of two hours to values of 1050°C and 30,000 PSI respectively. Inert argon gas was used as a buffer for the isostatic process. The samples were then held at these temperature and pressure for two hours before temperature reduction and gas ventilation over an additional two hours. The laser setup implemented was that of a standard linear z-fold bulk laser cavity as shown in Figure 4.

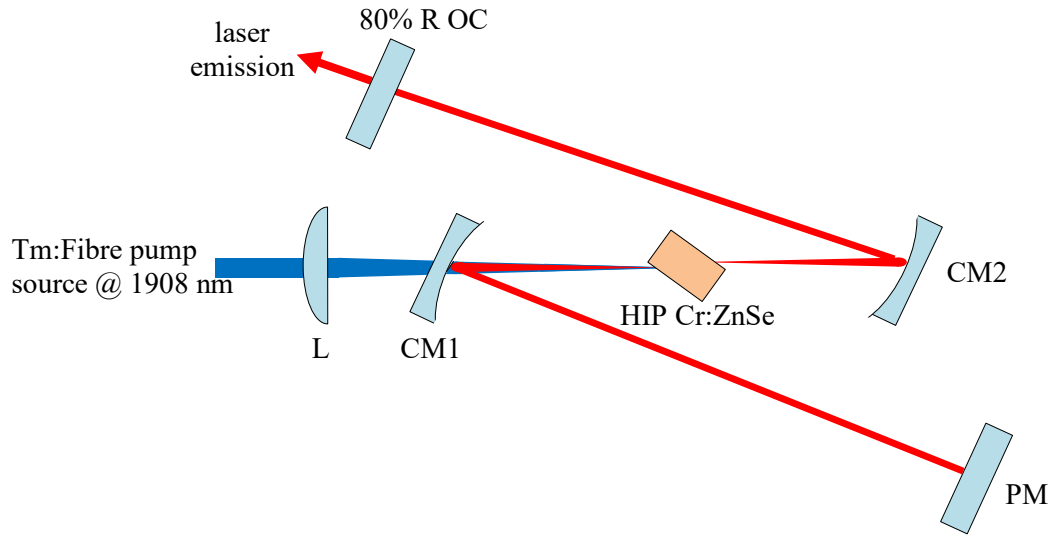

Figure 4. Schematic diagram of CW HIP Cr:ZnSe bulk laser pumped at 1.9 μm. L is a plano-convex 10 cm focal lens AR coated at 1.65 – 3 μm. CM1 and CM2 are plano-concave curved mirrors with 50 mm ROC and HR on the concave face for 2.3 – 2.8 μm, PM is a plane mirror HR for 2 – 3 μm and 80 % R OC is an output coupler which is 80% reflective for 1.7 – 2.7 μm.

The sample was placed at Brewster's angle at the focus between the plano-concave mirrors; CM1 and CM2, propagation occurred through the 7 mm length in order to maximise the gain. CM1 and CM2 set cavity folding angles of ~ 22° as this was the experimentally estimated angle which optimally compensated for the astigmatism imposed on the cavity by the Brewster angled faces of the crystal. The pump source is the same as that used in chapter 5; a 20W linearly polarised Tm:fibre laser operating at 1908 nm. The pump entered the cavity through the rear face of the CM1 and was focused into the laser crystal by the lens, L. The distance between both CM2→OC and CM1→PM is 12.5 cm, this distance arbitrarily chosen in this initial lasing attempt. The output coupler utilized was 80% reflective for 1.7 – 2.7 μm.

A graph of the HIP Cr:ZnSe bulk laser output power versus incident pump power is given in Figure 5. The power values were measured with the Spectra-Physics thermal power meter (model number 407).

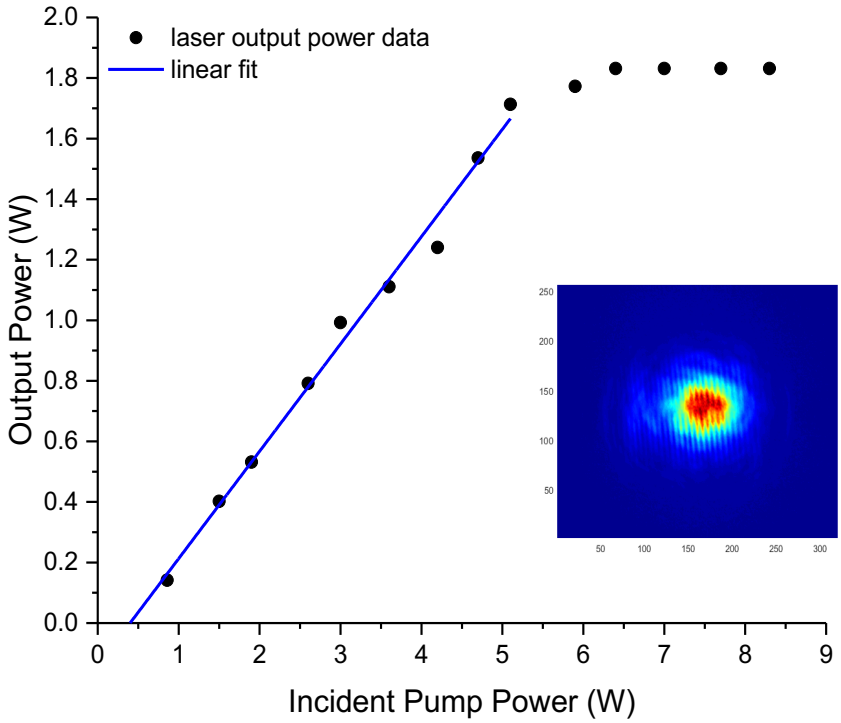

Figure 5. Graph of incident pump power versus output power of CW HIP treated Cr:ZnSe laser with an 80% R OC pumped at 1.9 μm. The inset image shows the far field output mode image in a 300 × 250 μm image.

The maximum output power observed was 1.83 W when pumped with 6.4 W, for output powers greater than this thermal rollover was observed as can be seen in Figure 6.7. There was no active cooling in place for the sample in the setup therefore, the addition of some cooling could improve the performance at higher pump powers > 6.4 W. Neglecting the last 5 data points in the region of thermal rollover, the laser has a slope efficiency of ~ 35.5% and lasing threshold of 399 mW. The inset image shows the far field output mode image which was observed with the FLIR SC7000 mid-IR camera to monitor the astigmatism imposed by the Brewster faces of the crystal. Note the vertical lines seen on the image are due to a stack of neutral density filters placed in the beam path to protect the camera detector from damage.

The spectral output of the HIP Cr:ZnSe laser was characterized with a Thorlabs OSA (OSA205) which has wavelength range: 1 – 5.6 μm and a resolution of 140 pm at the signal wavelength. The spectrum observed from the HIP Cr:ZnSe bulk laser can be seen in Figure 6, this spectrum was observed for a laser output power of 0.99 W when pumped with 3 W.

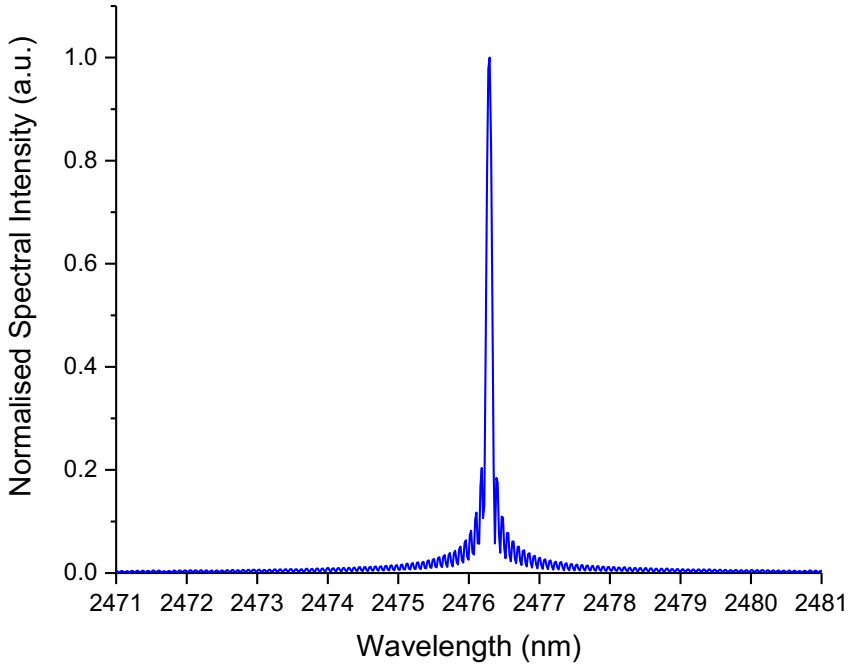

Figure 6. Normalised wavelength spectrum emitted by HIP treated Cr:ZnSe laser pumped with 1.9 μm. The measurement was taken at a pump power of 3 W and laser output power of 0.99 W.

The spectrum in Figure 6 is centred at ~ 2760.3 nm and has a FWHM linewidth of 140 pm limited by the resolution of the OSA. This linewidth is significantly narrower than the typical bandwidth emitted from free running Cr:ZnSe lasers reported in the literature. An example of the spectral emission from such a free running untreated Cr:ZnSe laser is shown in Figure 7. It has a FWHM linewidth spanning ~ 20 nm, thus proving the HIP treatment has significantly narrowed the spectral emission as expected by the results reported by Stites et al in [35].

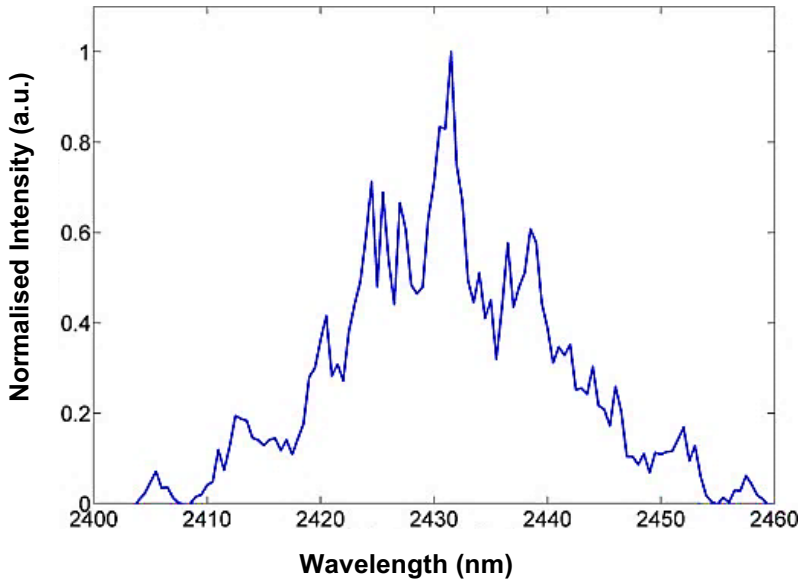

Figure 7. Broad spectral emission of a typical free running Cr:ZnSe bulk laser. Graph reproduced from [35].

This preliminary experiment confirmed that the HIP treatment had converted our sample from an inhomogenously to homogeneously broadened crystal. The next step of the work was to investigate HIP treated Cr:ZnSe for mode locking. In Politecnico di Milano the pump source available was a 1.57 μm Erbium doped fibre laser therefore the sample utilised for mode locking was initially characterised for CW operation with this pump. These results are presented in the following sub-section.

HIP treated Cr:ZnSe Laser pumped at 1.57 μm

The Cr:ZnSe sample to be investigated for mode locking had dimensions 2 × 3 × 7 mm with a dopant concentration of 1.05×10^{19} cm^{-3}, it was fabricated by IPG photonics then subsequently treated with HIP. The HIP Cr:ZnSe crystal was utilised in the linear x-fold bulk laser cavity shown in Figure 8. This x-shape was chosen over the z-shape utilised in the previous sub-section due to space constraints of the curved mirror mounts. For mode locking, the ultimate aim is to generate high PRFs thus we sought to minimise the cavity length by employing smaller focal length curved mirrors. The mounts would only fit to correctly compensate the astigmatism by using an x-fold shaped cavity.

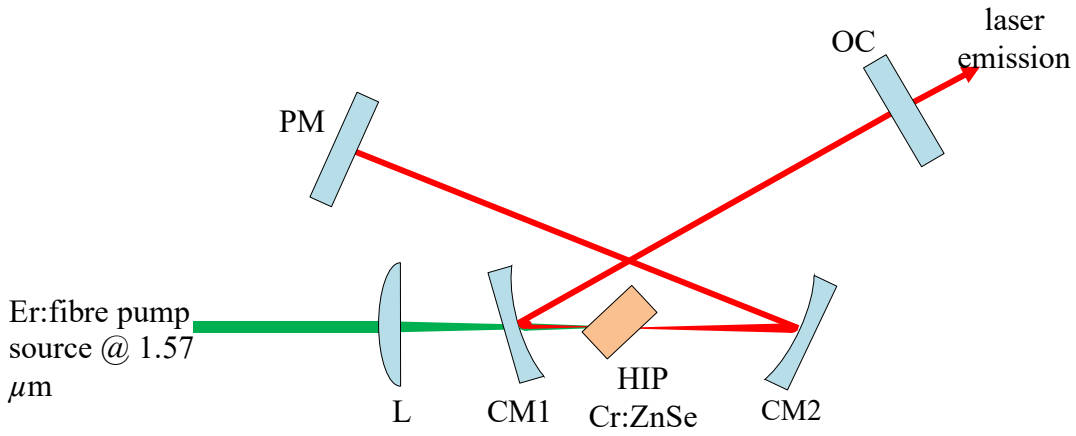

Figure 8. Schematic diagram of bulk laser cavity configuration for CW characterisation of HIP treated Cr:ZnSe pumped at 1.57 μm. L is a 50 mm focal length plano-convex lens AR coated for 1050 – 1700 nm, PM is a plane mirror which is HR for 2.3 – 2.6 μm and OC is the output coupler. CM1 and CM2 are plano-concave mirrors with ROCs of 30 and 50 mm respectively, both are HR for the signal wavelength.

The pump source in this case is a linearly polarised CW Er:fibre laser (IPG Photonics, ELR-LP-20), with maximum output power availability of 5.5 W. CM1 is a plano-concave mirror with a 30 mm radius of curvature (ROC) HR, > 99.5%, coated for the range 2.3 – 2.6 μm. CM2 is also a plano-concave mirror but has an ROC of 50 mm and is HR, > 99% from 2.3-2.8 μm. PM represents a plane mirror HR, >99.5%, for 2.3 – 2.6 μm and OC represents the output coupler. The sample is again placed at Brewster's angle relative to the input pump beam, at the point of focus between the plano-concave mirrors and the pump beam is focused into the crystal through CM1 with lens L. CM1 and CM2 set folding angles of 17° in both arms of the cavity, which is the angle calculated by numerical simulations, based on ABCD matrices, to compensate for astigmatism imposed on the cavity by the Brewster-angled surfaces of the crystal. The distance between CM2 →PM is 31 cm and from CM1→OC is 50 cm resulting in a total cavity length of approximately 85 cm. CM1 is not optimised for transmission of the pump wavelength through the rear face and allows transmission of 74%. This has been accounted for in the incident pump power levels quoted in the results. Propagation occurs through the 3 mm length of the crystal which was not actively cooled in this CW characterisation, therefore the pump power was limited to < 1 W to reduce any detrimental thermal effects on the laser performance. We characterised the power

performance of the laser with two different output couplers: one coated for 97% reflectivity at 2.05 – 2.43 μm (97% R OC) and one for 80% reflectivity for 1.7 – 2.7 μm (80% R OC). The CW laser output power versus the incident pump power for both OCs is displayed in Figure 9. Both were measured after propagation through a 2 μm long pass filter using a Thorlabs thermal power sensor with model number S401C, designed for detection in the wavelength range 0.2 – 10.6 μm.

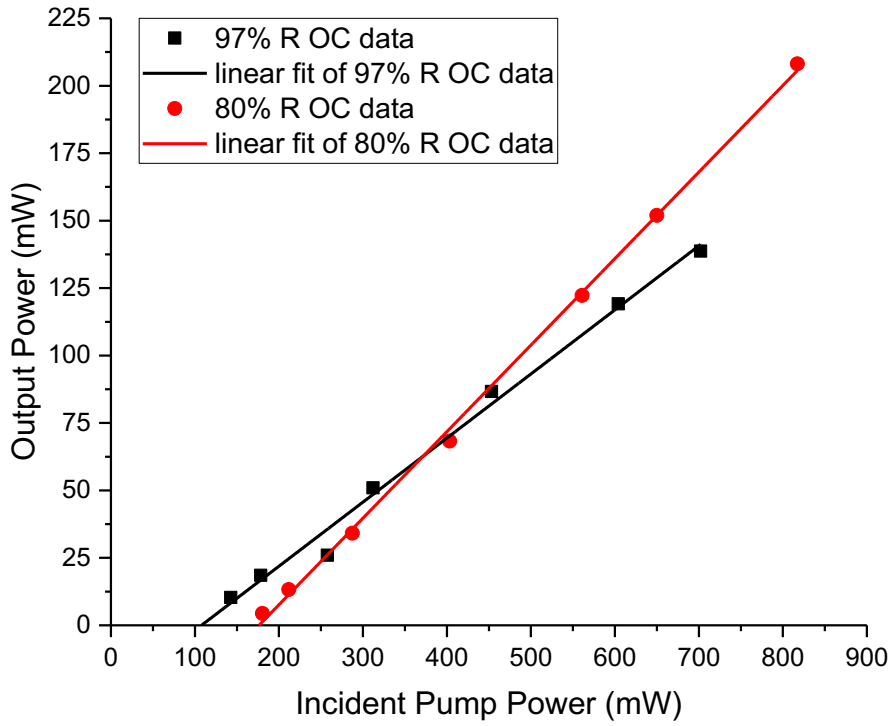

Figure 9. Graph of incident pump power versus output power of CW HIP treated Cr:ZnSe laser for 80% and 97% reflectivity output couplers.

With the 80% R OC the maximum output power was 208 mW measured for a pump power of 817 mW, the slope efficiency was 32% and the threshold was 177 mW. For the 97% R OC the laser threshold was 108 mW and the slope efficiency was 24%. The maximum output power obtained in this case was 139 mW for a pump power of 702 mW, it was decided not to increase pump power beyond this due to the lack of active cooling and increased intracavity power with this output coupler.

The wavelength spectrum emitted by the HIP Cr:ZnSe laser was measured with an extended InGaAs array near-IR spectrometer operating in the wavelength range from 0.9 – 2.55 μm, it was manufactured by Ocean Optics Inc. with model number

NIRQuest512-2.5. The normalised wavelength spectra measured with both output couplers are shown in Figure 10.

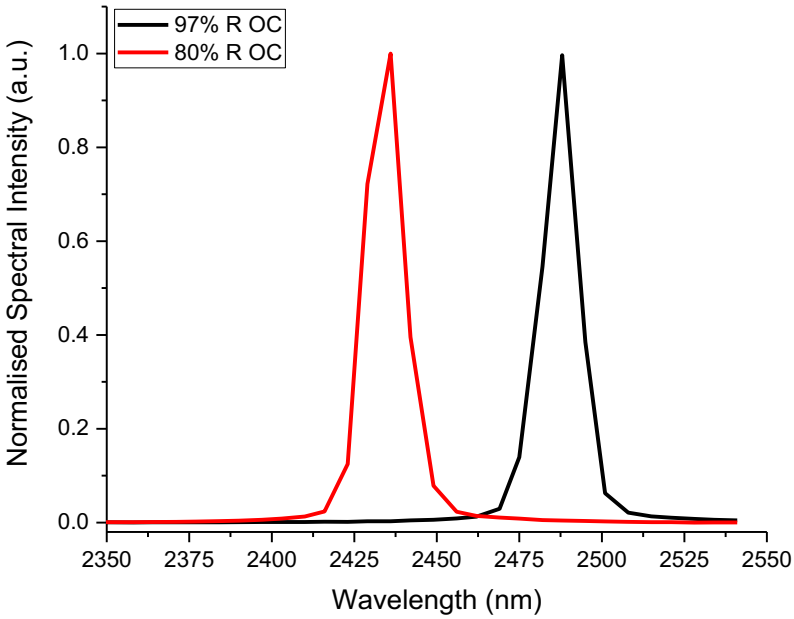

Figure 10. Normalised intensity wavelength spectra of HIP treated Cr:ZnSe laser pumped at 1.57 µm for 80% and 97% reflectivity output couplers.

As can be seen in Figure 10, the emission spectrum of the 97% R OC is centred at ~ 2488 nm, longer in comparison to the spectrum obtained with the 80% R OC which is centred at ~ 2436 nm. This shift may be due to the peak reflectivity being different for each of the coatings on the output couplers. It may also have a contribution due to the absorption of the Cr:ZnSe which extends into the emission cross section as can be seen in Figure 1. This means that for the higher R OC, the population inversion is lower and the peak gain wavelength is longer than the peak of the emission cross section. For the lower reflectivity OC, the ground state is less populated and thus the absorption is less, the peak gain wavelength is therefore closer to the peak of the emission cross section. The FWHM linewidth of the spectra are both ~ 14 nm which is considerably narrower than the typical bandwidth emitted from a free running Cr:ZnSe laser shown in Figure 7. In this case the measured spectra of the HIP treated sample are limited by the 7 nm resolution of the near-IR Spectrometer, it is expected that the true linewidth is much narrower in agreement with the sub-140 pm level demonstrated in Figure 6.

It is noted here that there is further evidence that the HIP conditions lead to narrowing of the linewidth in the spectral emission of TM:II-VI ULI waveguide lasers. The typical

spectral emission of a Cr:ZnSe ULI depressed cladding waveguide laser is demonstrated in Figure 11 a), whereas the spectral output of both a Fe:ZnSe ULI waveguide laser and bulk laser is shown in Figure 11 b).

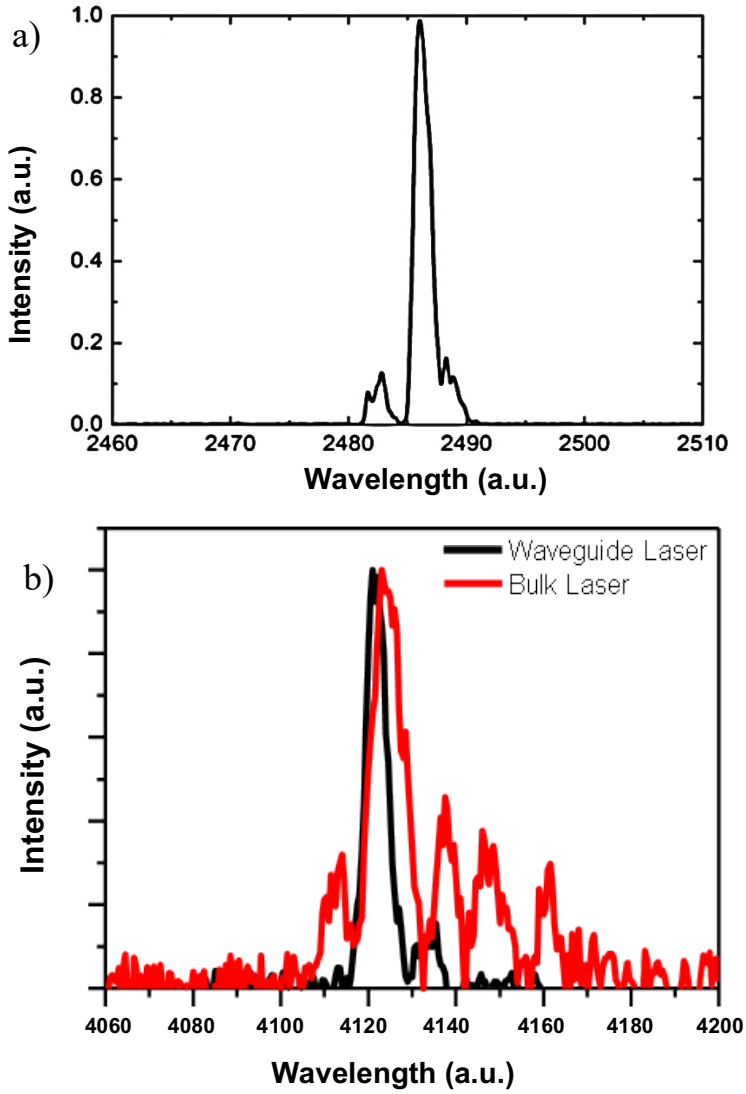

Figure 11 a) Typical spectral emission of Cr:ZnSe ULI waveguide laser. b) Spectral output both of Fe:ZnSe ULI waveguide laser and bulk laser. Images have been reproduced from [41] and [33] respectively.

The spectrum of the Cr:ZnSe waveguide laser in Figure 11 a) has a FWHM linewidth of 1.6 nm, this is a great deal narrower than the 20 nm FWMH linewidth of the free running bulk laser emission presented in Figure 7. Similarly, for the Fe:ZnSe lasers demonstrated in Figure 11b), the 6.7 nm linewidth emitted by the waveguide laser is narrower than the bulk counterpart which consists of multiple peaks spanning ~ 50 nm. From these results it has been proposed that the ULI process results in conditions

within the crystals which are consistent with HIP treatment. In fact, it has been calculated in [42] that ULI results in temperatures in excess of 1100°C and pressures ≈ 50,000 PSI at the irradiated focal region in the substrate, similar to those utilised in the HIP treatment in [35]. Therefore, it is believed that the ULI process also removes defects in the irradiated area of crystal hence leading to some narrowing of the spectral output [34].

After confirming that the emission from the HIP Cr:ZnSe bulk laser was spectrally narrowed as intended by the HIP treatment the laser was subsequently investigated for mode locked emission.

KLM Operation of a HIP Treated Cr:ZnSe Bulk Laser

KLM has found the majority of its success with Ti:sapphire as the active gain media. This has led to generation of ultrafast pulses with durations down to 5 fs in the near-IR extending over the range 600-1350 nm [43]. However, KLM is generally more difficult to achieve in the mid-IR because the Kerr effect is inversely proportional to laser mode size in the crystal, and this mode size itself is proportional to the square root of the signal wavelength. Thus at mid-IR wavelengths it is generally more challenging to induce the necessary Kerr effect for mode locking, expect for the case of sufficiently high nonlinear refractive index media [44]. For that reason Cr:ZnSe is particularly suitable for use in KLM, it has a n_2 value of ~ 7.5×10^{-19} m^2W^{-1} at 2.4 μm [45], around 25 times greater compared to $n_2 = 3 \times 10^{-20}$ m^2W^{-1} at the signal wavelength in Ti:Sapphire [46]. It can be seen in Table 5 that KLM used in combination with dispersive mirrors for GDD control has facilitated the generation of the shortest ultrafast pulses from a polycrystalline Cr:ZnSe laser. Therefore, this is the method which has been adopted here to investigate the potential for the emission of ultrafast pulses from HIP treated Cr:ZnSe.

A schematic diagram of the KLM HIP Cr:ZnSe laser cavity is shown in Figure 12. Although it is similar to that of the x-fold resonator used for which the CW characterisation, in this case the dispersion of the cavity elements must be considered.

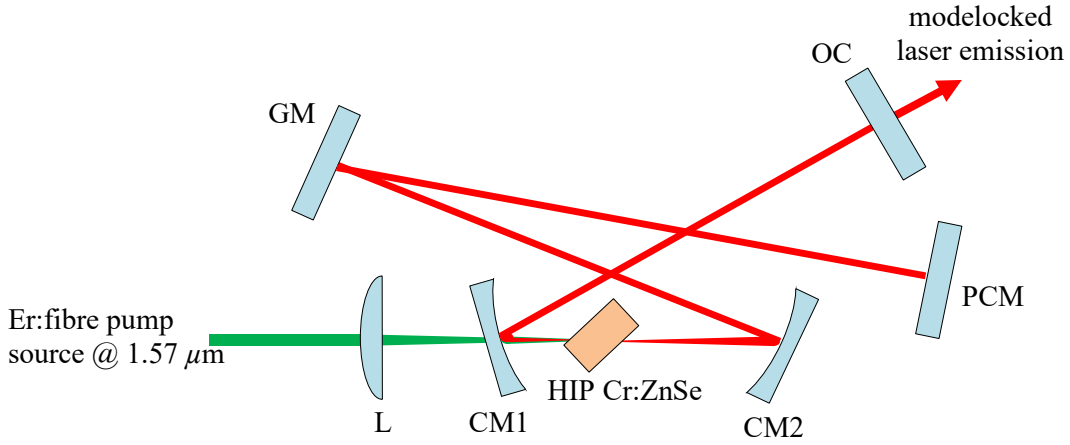

Figure 12. Schematic diagram of KLM HIP treated Cr:ZnSe Laser. L is a plano-convex 50 mm focal length lens. CM1 and CM2 are plano-concave mirrors with 30 mm and 50 mm ROCs respectively, both are HR for2.3 – 2.6 μm and PCM is a plane mirror with the same coating. CM1, CM2 and PCM are all chirped mirrors with GDD = ~ -250 fs².GM is plane gold mirror and OC is the output coupler.

L is the same 50 mm focal length plano-convex lens as in Figure 8. However, in this case CM1 and CM2 are plano-concave chirped mirrors with ROCs of 30 mm and 50 mm respectively. PCM is a plane chirped mirror which was mounted on a translation stage. The three chirped mirrors are coated for high reflectivity, > 99.5%, in the region 2.3-2.6 μm and have nominal GDD = - 250 fs². GM represents a plane gold mirror designed for low loss of typically < 2% in the mid-IR, and OC is the output coupler. The length of the cavity arms CM1→OC and CM2→GM→PCM was 36 cm and 42.5 cm respectively; resulting in a total cavity length of approximately 83 cm, as discussed further below this varies by a few mm depending on the separation of the curved mirrors which the mode locking is very sensitive to. The mode locked output was characterised utilising two output couplers with different coatings; one being 97% reflective for 2.05 – 2.43 μm (97% R OC) and the other was 99% reflective for 2.1-2.5 μm (99% R OC). In this case, the sample was actively cooled by securing on a copper heat sink held at a temperature of 20°C. This was achieved through the use of a Peltier-electric cooler, in which the heat was distributed by passive water cooling. The laser was pumped with the same Er:fibre source as in the CW characterisation. CM1 and CM2, again, set folding angles of 17° in both arms of the cavity to compensate for astigmatism imposed on the cavity. It was decided to propagate through the 2 mm length of the crystal for mode locking. This is because with chirped mirrors available, the GDD of the cavity could be compensated more fully through this sample

dimension than the other two. In this orientation the single-pass absorption of pump light was measured as ~ 69%.

The resonator was initially aligned for CW operation. Then the position of the curved mirrors and the crystal could be finely adjusted by use of the compact micrometer stages they were mounted on. This is necessary to identify the edges of the resonator stability regions as this is where KLM can most likely be achieved, a detailed discussion of the laser stability regions can be found in [47]. KLM operation was initiated by sharp translation of the PCM. It was found that KLM operation was not particularly difficult to start and the mode locked emission was extremely stable over several hours. Various measurements were made to fully characterise the mode locked laser performance which will now be detailed.

Mode locked operation was verified by detection of the laser output with a 1 GHz extended InGaAs photodiode connected to an oscilloscope. The photodiode was manufactured by Hamamatsu with model number G8423-03SPL and designed for use in the range 1.2-2.6 μm. The spectrum of the emitted pulses was measured with a near-to-mid-IR monochromator with gratings covering 0.8-20 μm manufactured by Newport (model number 74125). The measurement was taken with a resolution of 2 nm and slit aperture 0.28 nm. An interferometric autocorrelation measurement was taken to characterise the temporal duration of the pulses. The autocorrelator employed was a homemade setup based on 2-photon absorption in an InGaAs photodiode with a cut-off wavelength of 1.7 μm. The mode locking threshold and average output power performance of the laser was also measured. These measurements were recorded for both the 97% and 99% R OCs, the full results will be presented in Figures 13-19 with the discussion to follow.

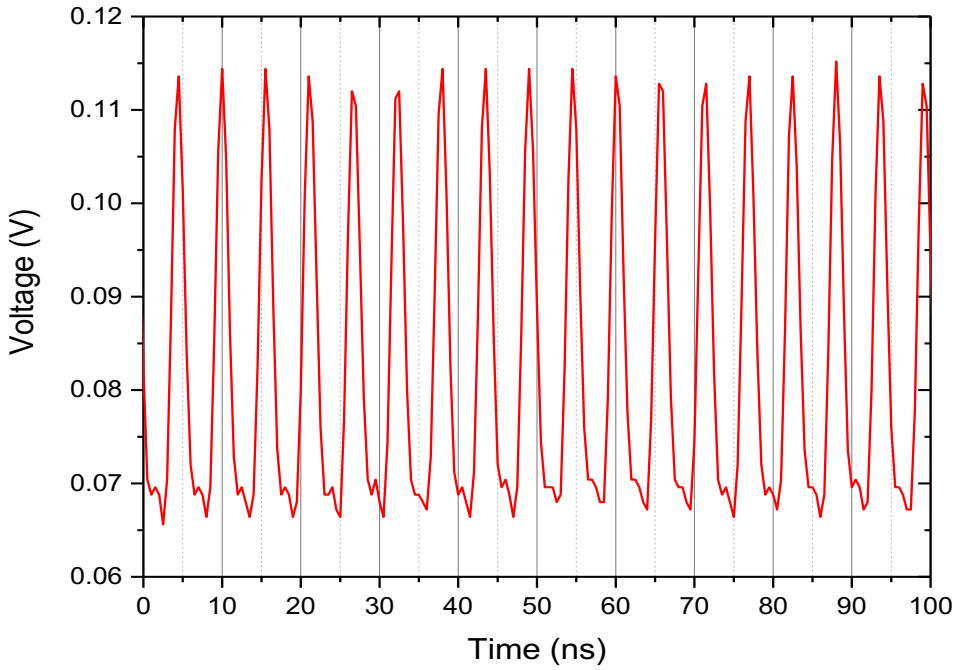

Figure 13. Mode locked pulse train emitted from HIP Cr:ZnSe laser with 97% reflective OC viewed with an oscilloscope.

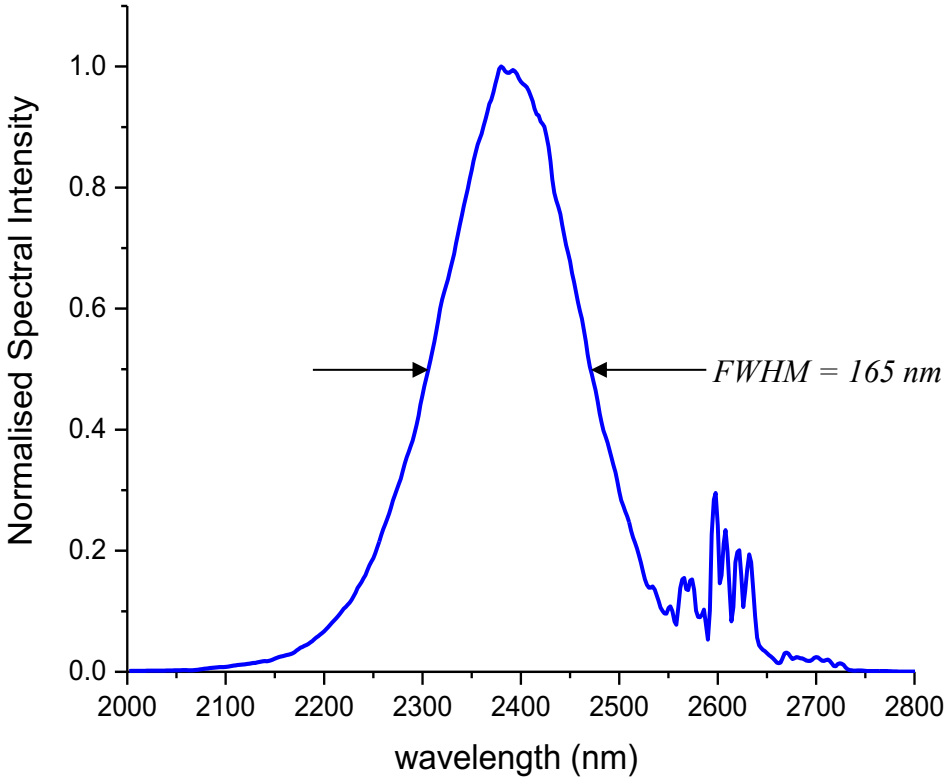

Figure 14. Wavelength spectrum of mode locked HIP Cr:ZnSe laser with 97% reflective OC. The spectrum is centred at 2388 nm with a FWHM of 165 nm.

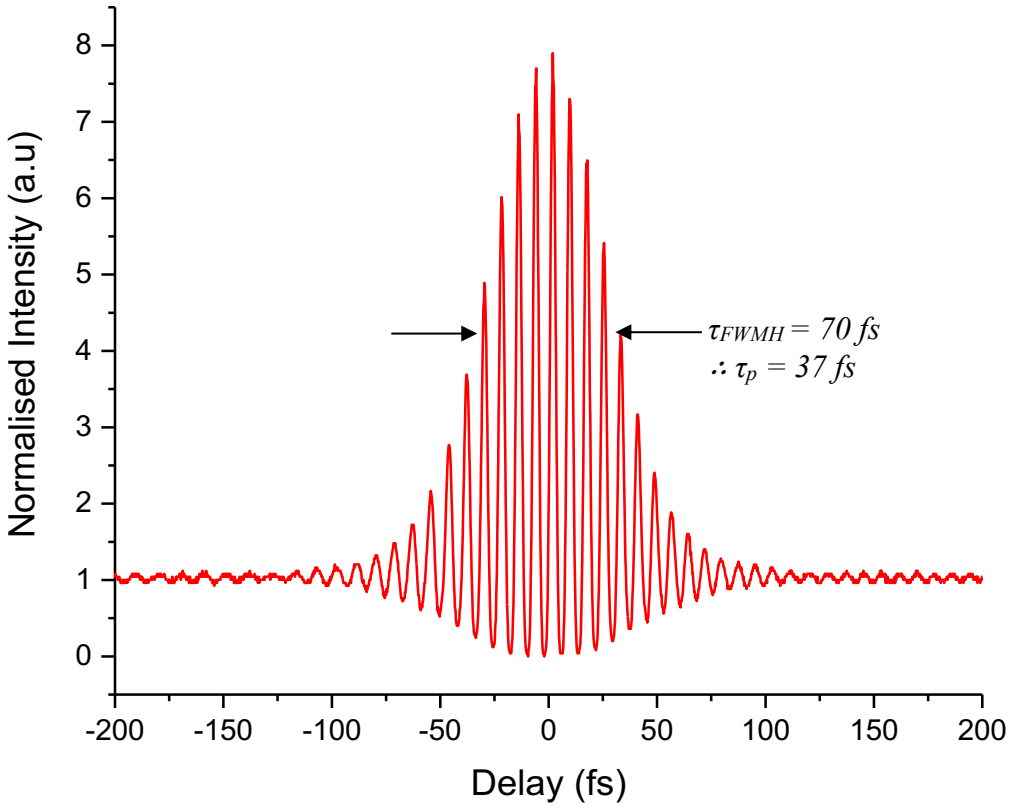

Figure 15. Interferometric autocorrelation trace of mode locked HIP Cr:ZnSe laser with 97% reflective OC, the FWHM of the trace is 70 fs translating to a pulse duration of 37 fs.

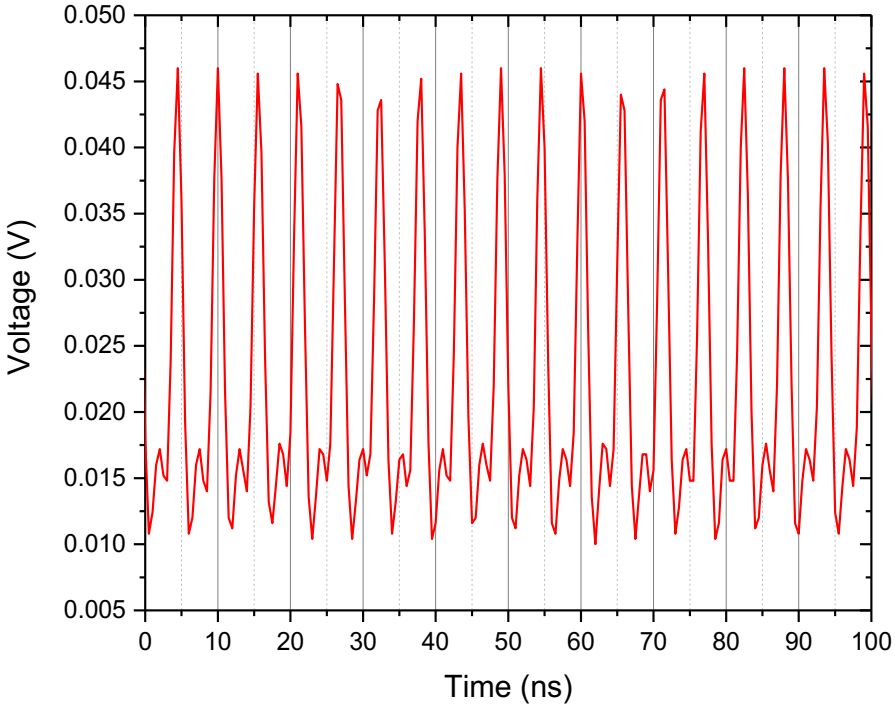

Figure 16. Mode locked pulse train emitted from HIP Cr:ZnSe laser with 99% reflective OC viewed on an oscilloscope.

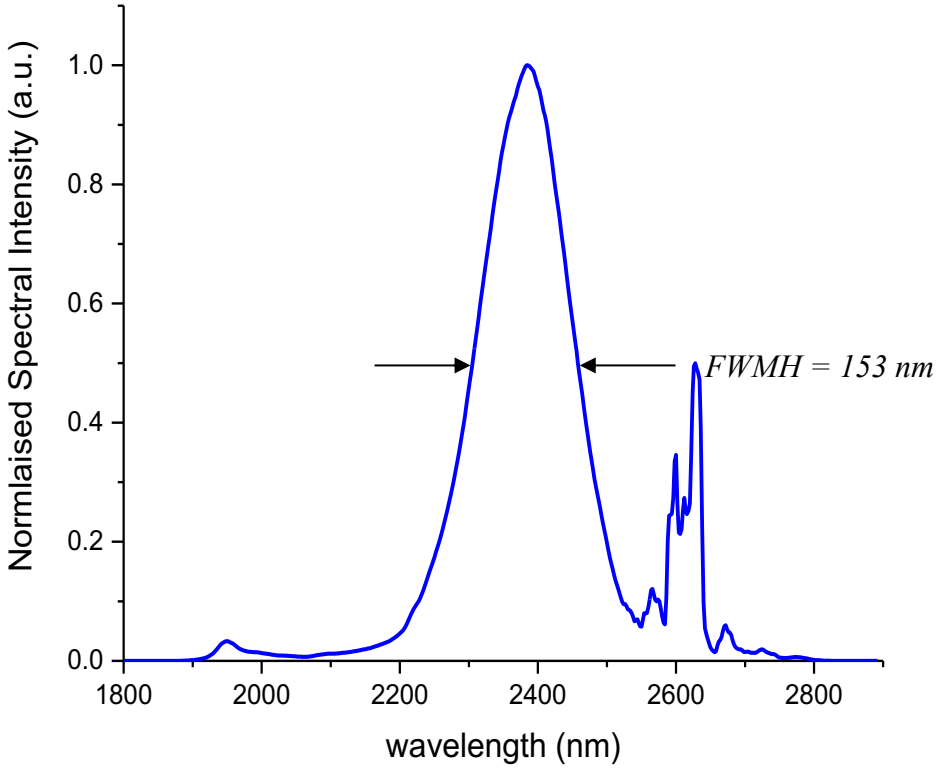

Figure 17. Wavelength spectrum of mode locked HIP Cr:ZnSe laser with 99% reflective OC. The spectrum is centred at 2382 nm with a FWHM of 153 nm.

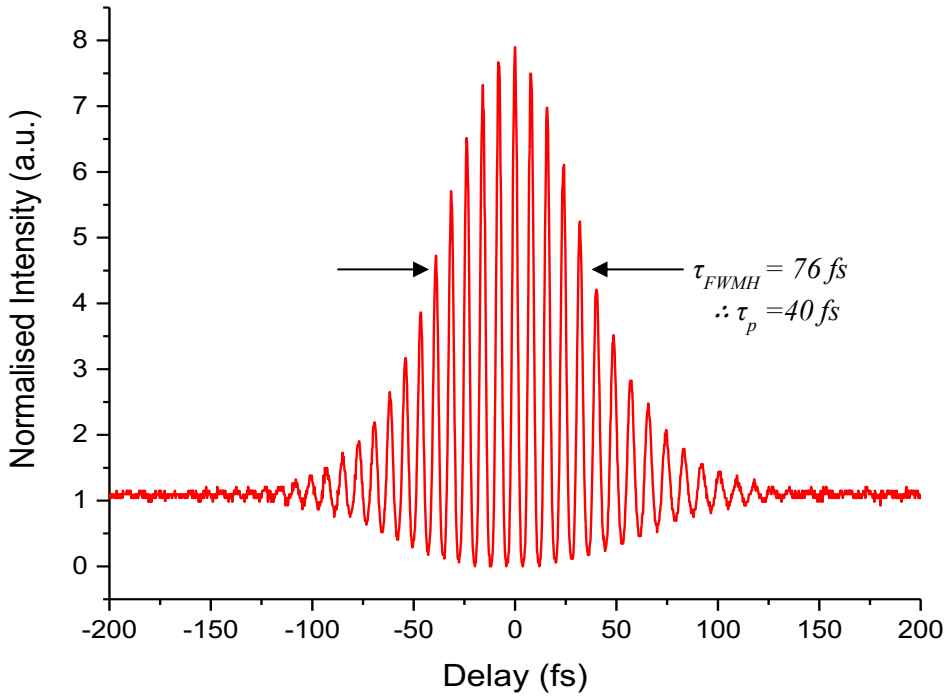

Figure 18. Interferometric autocorrelation trace of mode locked HIP Cr:ZnSe laser with 99% reflective OC, the FWHM of the trace is 76 fs translating to a pulse duration of 40 fs.

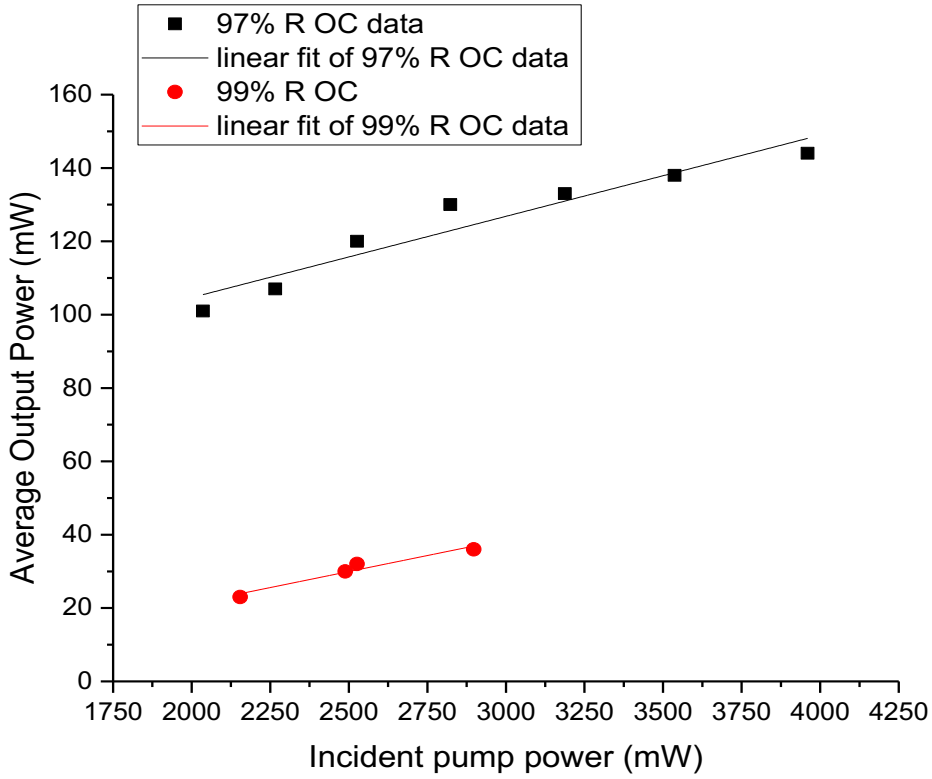

Figure 19. Average output power versus incident pump power of mode locked HIP Cr:ZnSe laser.

Figures 13 and 16 contain the mode locked pulse trains emitted for the 97 and 99% R OCs respectively. In Section 4.1 is was presented that the expected PRF of a mode locked laser can be estimated using $\frac{c}{2nl}$, where c is the speed of light, n is the intracavity refractive index and l is the cavity length. In the HIP Cr:ZnSe laser the index of the cavity is taken to be 1 as the majority of the propagation is in free space. The cavity length is ~ 83 cm which remained the same for both OCs, resulting in an estimated PRF of 181 MHz. As can be seen in Figures 13 and 16 the pulses are emitted with a period of approximately 5.5 ns hence a PRF of ~ 182 MHz, corresponding well with the expected value.

The wavelength spectrum obtained with the 97% R OC is shown emission in Figure 14, it is centred at 2388 nm with a FWHM of 165 nm. Note that there are a series of spikes observed in the long wavelength wing of the spectrum around 2.6 μm, these are due to water vapour absorption in the atmosphere common for spectra in this wavelength range in cavities which are not actively purged [48]. The corresponding interferometric autocorrelation trace for this OC shown in Figure 15 is characterised by the expected 8:1 peak-to-background ratio, and has a FWHM of 70 fs. Assuming a sech^2 pulse profile thus applying a deconvolution factor of 1.897, this translates to a pulse duration of 37 fs. The associated time-bandwidth product is therefore 0.321.

For the case of the 99% R OC, the wavelength spectrum is shown in Figure 17, it is centred at 2382 nm and has a FWHM spanning 153 nm. The spikes at ~ 2.6 μm are again present, but in this case there is also a low intensity spike at around 1950 nm which is not observed with the 97% R OC. The presence of this spike is most likely due to modulations in the reflectivity coating of this OC at ~ 1950 nm. The interferometric autocorrelation measurement obtained is shown in Figure 18, the trace again has the correct peak-to-wings ratio of 8:1 and in this case the FWHM is 76 fs corresponding to a pulse duration of 40 fs. The time-bandwidth product is calculated again assuming a sech^2 pulse profile, the calculated value is 0.323.

The obtained time-bandwidth products are slightly larger than the expected value of transform-limited sech^2 pulses of 0.315. This indicates there is a residual chirp in the pulses. To identify the reason for this chirps the net GDD of the cavity was estimated as follows: Brewster's angle for the Cr:ZnSe crystal is ~ 68° resulting in a propagation length through the sample of 2.16 mm and the GVD of ZnSe at the signal wavelength

of ~ 2385 nm is +209 fs^2mm^{-1} [49]. This results in a calculated total GDD of +903 fs^2 per round trip due to the laser crystal in the cavity. Data provided by the chirped mirror suppliers gives a GDD value of -220 fs^2 per bounce at the signal wavelength, thus a total round trip GDD due to the chirped mirrors is calculated to be $-220 \times 5 = -1100$ fs^2. The GDD of the gold mirror is zero, that of the atmosphere and the unknown value of the output coupler are assumed to be negligible in this estimation. From these calculations the net round trip intracavity GDD is estimated to be -197 fs^2, therefore in the anomalous dispersion regime. Furthermore, before arriving at the autocorrelator for the measurement the laser emission propagates through the 6.4 mm fused silica material of the OC and a 0.4 mm Germanium plate included in the beam path to filter out any SHG signal in the output. The GDD values for these components are ~ -1330 fs^2 for the OC and ~ +930 fs^2 for Ge resulting in an additional chirp of -400 fs^2. Therefore, there is indeed a negative chirp which acts to distort the pulse profile.

The mode locked laser average output power vs incident the pump power is displayed in Figure 19 for both of the output couplers. The 97% R OC results in a slope efficiency of 2.21% and the CW mode locking was found to be initiated at a minimum pump power of 2.04 W. The maximum average output power measured was 144 mW for a maximum incident pump power of 3.96 W, this is limited only by the available pump power. In the case of the 99% R OC the slope efficiency and CW mode locking threshold are 1.75% and 2.15 W respectively. The maximum average power for the 99% R OC was 36 mW measured for 2.9 W of pump power, for values greater than this the mode locking was very unstable and the average output power was observed to decrease. This is likely due to thermal issues in the crystal, more efficient cooling may improve the stability for these higher pump power values. Just below the mode locking threshold for both OC's the laser output was found to be continually switching between a Q-switched mode locked regime and CW emission with unstable output power and it was found that it could not emit stable CW emission without considerable changes to the curved mirror/crystal positions. This is not unexpected as the laser is aligned near the edges of the stability regions for KLM operation.

It may be logically expected that the higher reflectivity output coupler would result in a lower CW mode locking threshold due to higher expected intracavity energy, however this was not the case. However, the difference in the thresholds of ~ 110 mW

is relatively small compared to the pump powers applied, ranging 2-4 W. As the laser is operating on the edge of a stability region the intracavity losses are expected to be relatively high compared to in the case of operating will within the stability region. To obtain a clearer view of the effect the OC reflectivity value has on the mode locking threshold, it would be useful to repeat the measurements with lower reflectivity OCs. This was attempted with a 90% reflectivity OC but it was found that this was not sufficient to initiate KLM, therefore a higher value, e.g. 95% is required, but such a mirror was not available at this time.

The emitted mode locked pulse durations of 37 fs and 40 fs corresponding to 4.6 and 5 optical cycles are the shortest observed to date from a Cr:ZnSe crystal. The 97 % R OC led to the generation of slightly shorter pulses thus a broader spectral bandwidth. This is could be due to a slightly broader bandwidth of the reflective coating on this OC compared to the 99% R OC, the reflective coatings of the two OCs would have to be analysed to confirm this. These record results indicate that the HIP treatment is advantageous for mode locking of polycrystalline Cr:ZnSe lasers. During the HIP treatment the crystal is converted from inhomogeneously to homogeneously broadened material, the reasons that this can be beneficial for ultrafast pulse generation will now be discussed. In an inhomogeneously broadened laser material, if the photon interaction time of propagating photons is less than the thermalisation time, the energy cannot be redistributed across the gain spectrum at sufficient speed, this results in any oscillating laser pulse burning a hole in the gain spectrum [50]. This reduces the overall gain and leaves much of the excited state energy inaccessible to the building laser pulse. During the initiation of mode locking whilst the pulse begins to form, if the pulse duration falls below that of the thermalisation time the pulse compression process stalls, hence the duration is limited to the equivalent of the thermalisation time. In polycrystalline solid- state crystals such as ZnSe, this is of the order of ~ 100s of fs where thermalisation is determined through the phonon spectrum, as a result the generation of few-cycle pulses can be difficult to achieve. HIP treatment of the polycrystalline material has two major effects 1) the removal of crystalline defects and 2) growth of the grains. The removal of defects means that all ions now experience the same crystal fields, thus the crystal now acts as a homogenously broadened material. In combination with this defect removal, fewer grain boundaries reduces the phonon lifetime so even if the material is not perfectly

homogeneously broadened the thermalisation time is reduced in any residual inhomogeneously broadened fraction [34, 35]. Homogenous broadening results in no such spectral hole burning and the gain profile is uniformly depleted as the pulse builds. Any residual inhomogeneously broadened component has very small thermalisation times and so the mode locked pulse can still access the full gain spectrum. Of course net intracavity dispersion also has major consequences on resultant pulse duration. However, the results presented in this section strongly suggest that the laser is operating in a regime in which the thermalisation time is less than the photon interaction time i.e. the pulse duration, and as such has allowed for the generation of record short sub-40 fs pulse durations.

Future Work

The next stage of our work in this material will focus on initially testing the KLM cavity with the available 1.9 μm pump source. It is expected that this will result in improved output power performance because of the reduced quantum defect and the fact that the absorption peak in Cr:ZnSe is closer to 1.9 μm than 1.57 μm as can be seen in Figure 6.2. In addition to this, the quantum defect is reduced for a 1.9 μm also resulting in higher obtainable slope efficiencies. The cavity will subsequently be optimised for GHz PRF emission whilst maintaining the ultrafast sub-ps pulse width. This would satisfy the aim of developing a GHz PRF ultrafast mid-IR emission source which also has high power capability.

Summary

We have presented results of an ultrafast HIP treated Cr:ZnSe laser. Two different HIP treated Cr:ZnSe crystals were initially characterised for CW laser operation. These experiments were carried out separately in HWU and Politecnico di Milano utilising 1.9 μm and 1.57 μm pump sources respectively. The laser crystals were both utilised in astigmatically compensated bulk resonators and the pump powers were intentionally kept low during these measurements due to an absence of active crystal cooling. In both experiments the laser exhibited a significantly narrower spectral emission linewidth than traditional free running polycrystalline Cr:ZnSe lasers which typically span 10s of nm. The emitted FWHM linewidths were 140 pm and 14 nm when pumped with 1.9 μm and 1.57 μm respectively. In the latter case this was limited by the spectral resolution of the different spectrometer used and it is expected that the true linewidth

is sub-nm as in the former case. The spectral narrowing is a result of the HIP treatment converting the Cr:ZnSe crystals from an inhomogenously to a homogeneously broadened material as demonstrated first by Stites et al. [35].

The laser was then operated in an ultrafast pulsed regime through the technique of KLM. The cavity was similar to that for the CW experiments with the addition of chirped mirrors for management of the intracavity dispersion and plane gold mirror to control the cavity length. Mode locked emission was initiated by sharp perturbation of one of the intracvaity chirped mirrors. Stable CW-mode locked operation was observed for 97% and 99% R OCs. With the 97% R OC the temporal pulse duration was found to be 37 fs with a spectral bandwidth of 165 nm centred at 2385 nm. For the 99% R OC the pulse duration was 40 fs and the bandwidth was 153 nm centred at 2382 nm. The slightly shorter pulse duration obtained with the former is likely due to the broader bandwidth of the reflective coating on the OC. The 97% R OC also exhibited superior power performance; demonstrating an average output power of 144 mW when pumped with 3.94 W, compared to a maximum of 32 mW for the 99% R OC which could not be pumped with more than 2.9 W due to thermal instabilities. A PRF of 182 MHz was measured corresponding well with the 83 cm cavity length. These results represent the shortest pulse duration to date generated in a Cr:ZnSe laser, indicating that HIP treatment of the crystal may be beneficial for the emission for ultrafast sub-ps pulses in this medium. The next stages of this work are to characterise the mode locking performance when pumped at 1.9 μm and optimise the cavity length for GHz PRF.

Single pass ultrafast Cr:ZnSe waveguide amplifier preliminary results

High average power, ultrafast 2-3 μm laser pulses are essential for various applications such as high harmonic generation, time resolved studies and the development of high power mid-IR frequency combs for sensing and spectroscopy [51-53]. The thermal limitations imposed on Cr:ZnSe crystal restrict the output power capability of this laser material. This effect becomes particularly detrimental in high PRF lasers as the application of active cooling for effective heat distribution is difficult to achieve in such small resonators. Although Cr:ZnS has better thermal properties in comparison, there have been no reports of significant improvement in the output power of this material

compared to Cr:ZnSe. Therefore, in summary it is challenging to generate multi-Watt level GHz PRF ultrafast pulses from Cr:ZnSe/ZnS lasers.

One solution is to utilise a ULI waveguide amplifier. The implementation of a waveguide geometry guarantees a high degree of overlap between the pump and signal due to the tight confinement, resulting in a very compact and robust high gain amplifier. A single pass waveguide amplifier experiment was undertaken to explore this method. The preliminary results of this investigation will now be presented here. Depressed cladding waveguide structures were fabricated in a 3 × 6 × 7 mm Cr:ZnSe sample by ULI, for clarity it is noted that this sample was not HIP treated. The sample was fabricated by IPG photonics with a dopant concentration of 6 × 1018 cm-3. The waveguides were inscribed by our collaborators in the AFRL in Ohio, USA. The inscription laser was a Yb:fibre laser (IMRA μJewel model D1000) operating with linear polarisation at a central wavelength of 1047 nm with a pulse width of 450 fs and a PRF of 100 kHz. The pulses were focused by a 0.68 NA lens to inscribed the waveguides at a depth of ~ 200 μm beneath the surface of the sample. A set of 24 waveguides were fabricated in the 7 mm length of the sample with an average laser power of 120 mW at a translation speed of 10 mms-1. The waveguide diameters decreased in increments of 5 μm between 100 – 45 μm, two waveguides were written at each diameter with 1 overscan in the first and 2 overscans in the second. These waveguides were originally fabricated to be pumped at 1.9 μm for laser emission; previous investigations had identified these as optimum parameters for this application. After inscription the input and output facets had been AR coated for 1.9 – 3 μm for the mitigation of Fresnel reflection losses. The sample was then utilised in the counter-propagating amplifier setup in Figure 20.

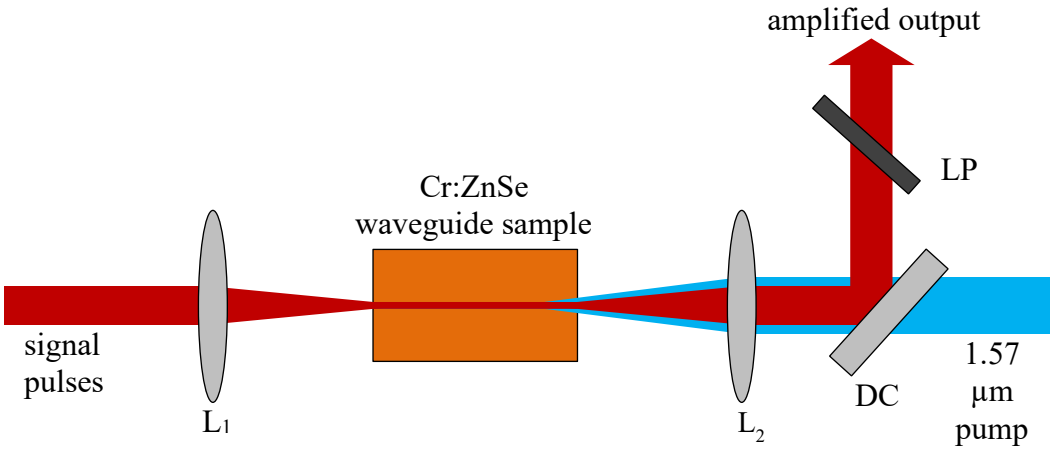

Figure 20 . Schematic of Cr:ZnSe ULI waveguide amplifier. L_1 and L_2 are 50 mm focal length plano-convex lenses AR coated for 1.65 - 3µm and 1.05 – 1.7 µm respectively. DC is a 45° dichroic HR on the front face for 2 – 3 µm and AR on the rear for the1.57 µm pump wavelength. LP is a 2 µm long pass filter.

In the setup the ultrafast signal pulses were provided by a KLM Cr:ZnSe laser operating at 2.4 µm with an average output power of 110 mW measured behind L1 and a PRF of 140 MHz. The input pulse duration and bandwidth are 47 fs and 160 nm respectively. The pulses were coupled into the waveguides with L1 which is a plano-convex 50 mm focal length lens AR coated for 1.65 – 3 µm. The pump source was the same Er:fibre laser that pumped the KLM HIP Cr:ZnSe in chapter 6, the maximum power availability in this case was 10.25 W. It was coupled into the waveguides in a counter-propagating direction to the signal pulses with L2, which is a plano-convex 50 mm focal length lens AR coated from 1050 – 1700 nm. DC represents a 45° dichroic mirror which allowed propagation of the pump light through the rear face and is HR on the front face for 2 – 3 µm. LP is a long pass 2 µm filter to remove any residual back reflected pump, as the AR coating on the end facets was not applied for this pump wavelength. Initially, the maximum pump power was coupled into each waveguide and the amplified output power was measured after the LP filter. The waveguide which resulted in the maximum amplified signal had a 90 µm diameter and was written with one overscan. The emitted signal from this waveguide with no pump power applied was measured as 80 mW. When pumped with the maximum pump power of 10.25 W at 1.57 µm, the amplified output had measured power of 430 mW. This translates to an internal gain factor of 5.375. In terms of the overall system efficiency from input to output signal, the gain factor is ~ 3.9. The spectral emission was measured with the

same NIRQuest512-2.5 spectrometer that was used for the spectra taken in sub-section 6.2.2; it operates in the range 0.9 – 2.55 μm with a resolution of 7 nm. These measurements for the case of no pump and maximum power applied are shown in Figure 21 a) and b).

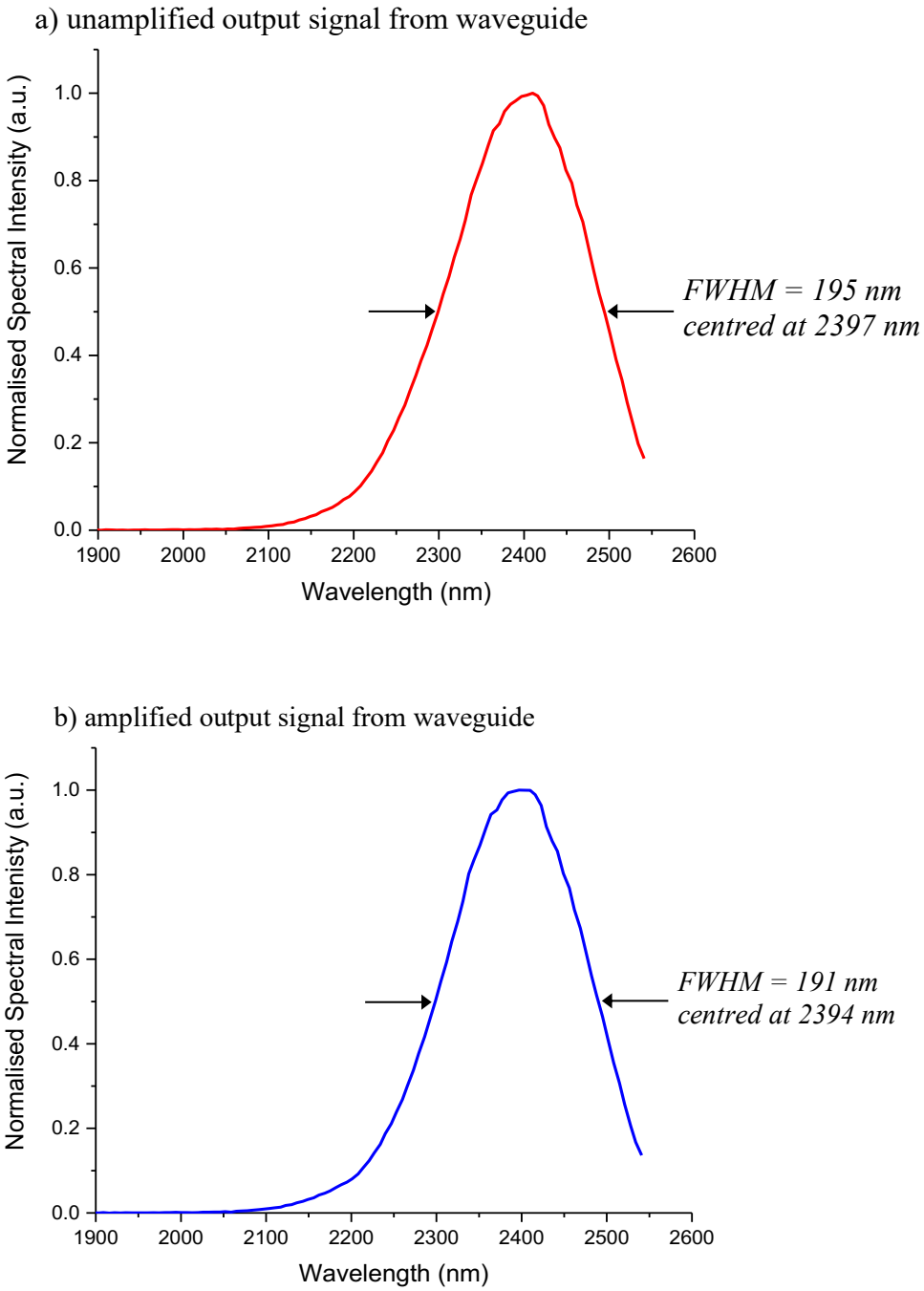

Figure 21. Spectral emission from Cr:ZnSe waveguide amplifier setup with a) no pump and b) 10.25 W of pump applied. The spectrum in a) is centred at 2397 with a FWHM of 195 nm, the spectrum in b) is centred at 2394 nm with a FWHM of 191 nm.

The spectra cut off at 2.55 μm as this is the upper limit of the spectrometer operational range.

Figures 21 a) and b) indicate that the waveguide does induce spectral broadening in the pulses. The input signal pulses have a 47 fs pulse duration and a FWHM bandwidth of ~ 160 nm, which has been broadened to > 190 nm in the waveguide. Going forward, temporal pulse durations are required to confirm the implied pulse compression imposed by the waveguide. The spectral measurements also demonstrate that when the waveguide is pumped the spectral output is narrowed very slightly, by ~ 3 nm, further research is required to confirm and understand the source of this narrowing. The gain measurement was also repeated in the bulk material of the sample by simply translating the sample away from the waveguide region and optimising the lens positions for the maximum amplified output signal. The internal gain factor in the bulk was measured to be 3.8, and the overall system gain factor recorded was ~ 3. It would also be useful in the future to measure the spectral emission and pulse duration after propagation through the bulk material to provide a comparison of the nonlinearity with the waveguide. It is evident from this experiment that the waveguide amplifier is indeed advantageous in the amplification of ultrafast pulses compared to the bulk. It is expected that the gain obtained could be improved further by optimising the coupling of the pump light as this was not done in our setup.

Future Work and Summary

This experiment was conducted to provide an initial indication of the amplification of ultrafast pulses in a Cr:ZnSe ULI waveguide. In summary, this preliminary investigation has shown that a Cr:ZnSe ULI waveguide is a promising candidate for the amplification of ultrafast pulses from Cr:ZnSe/ZnS lasers. Thus providing a solution to the output power limitations associated with these lasers. There is a plethora of work to be done, to further investigate and optimise the setup in terms of both output power and spectral broadening. We anticipate that tighter confinement imposed by a smaller diameter waveguide may induce larger nonlinearity in the gain medium to broaden the spectral output and thus compress the pulses. The long term goal is to implement the GHz KLM mode locked HIP Cr:ZnSe arrangements with a waveguide amplifier. The result will be a compact, robust, mid-IR, few-optical-cycle, high PRF emission source, with Watt-level output power capability.

Waveguides Modelling in Cr:ZnSe for Kerr-Lens Mode Locking

Introduction

For the realisation of ultrafast laser pulses from a Kerr-Lens Mode-locked laser, two designs consisting of a channel waveguide and a coupled channel waveguide in Cr:ZnSe is proposed and tested for suitability using RSoft™ Photonic Device Tools. Initially self-trapping and self-focusing were tested in bulk Cr:ZnSe, before the two waveguide geometries were evaluated with similar parameters. The waveguides were shown to possess lower critical powers and good levels of self-focusing, while the coupled waveguides displayed low loss and critical powers similar to the standard waveguide. These results point towards the possibility of such devices being used for Kerr-lens mode locking.

Cavities for KLM

Experimental

An important factor for evaluating a suitable cavity for KLM is the Kerr-nonlinear strength. This parameter gives an indication of the level of self-amplitude modulation that occurs within a resonator. It is defined as the change in beam waist size at some plane within the cavity due to self-focusing caused by the optical Kerr effect at low powers[45].

$$\gamma = \left(\frac{1}{w}\frac{dw}{dP}\right)_{P=0} \tag{1}$$

where w is the beam waist and $P = P/P_{cr}$. A negative value shows that for larger intensities, a smaller spot size is obtained. A negative value is necessary for KLM and for large enough numbers, it can be self-starting. Both small and large negative γ values are usually obtained at regions near the edge of cavity stability, where the beam is tightly focused within the medium [54]. These regions can be determined analytically, using complex nonlinear ABCD matrices [55]. Usually by deciding on a cavity and varying certain parameters such as the position of the gain medium and mirror distances, the Kerr nonlinear strength can be established at certain points in the cavity, for different stability zones. From this, positions where KLM can be sustained are found. This type of analysis has been carried out for many types of

cavities, from typical Z and X folded cavities to linear three element cavities. Z and X cavities have seen much success with KLM due to the fact that the medium can be Brewster cut to avoid reflection losses, and there is flexibility in design due to the multiple parameters that can be changed. Typical designs can be seen in figure 9. Usually, KLM is achieved by tapping one of the mirrors to induce the self-focused beam.

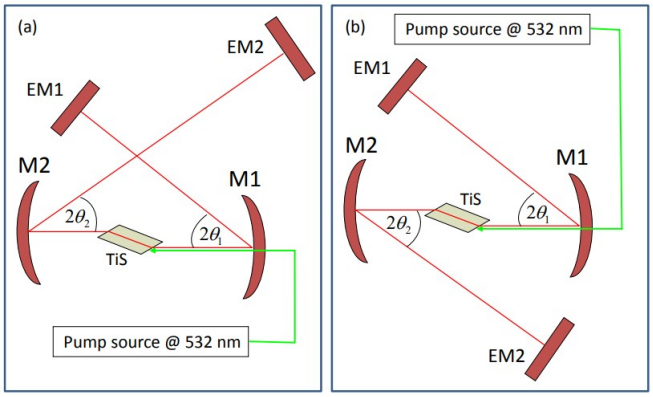

Figure 22: Standard X and Z cavities for KLM, with Ti:S gain medium. Diagram reproduced from ref. [54]

To the best of our knowledge, KLM has never been achieved in a waveguide geometry. Hence typical cavities such as the X or Z fold may not be suitable for such a device. One of the reasons for using a waveguide would be to drastically reduce the cavity length, potentially by butt-coupling two planar mirrors to the ends of the waveguide. Therefore, a more compact cavity should be sought to fit with the nature of the waveguide.

One such cavity is a compact three element cavity, a generalised version shown in figure 10. This cavity saw much interest in the years following the initial demonstration of KLM due to its self-starting capabilities and high repetition rates [56]. This type of cavity has recently been used to generate very high repetition rates of > 20GHz [57], and could be promising for a waveguide as the length can be made very small compared to Z and X cavities. It also has several regions which support both hard and soft aperturing [58].

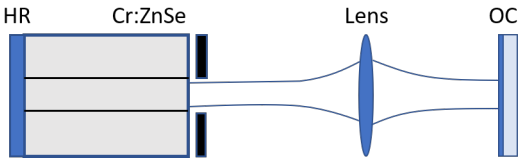

Figure 23: Proposed compact three element cavity for KLM. Shown is Cr:ZnSe gain medium with inscribed waveguide and hard aperture at the face of the crystal

Rsoft BeamProp Software

BeamPROP is a beam propagation software focused towards simulating the movement of light waves within waveguides. It operates using complex finite-difference techniques to solve the paraxial and parabolic approximations to the Heimholtz equation. BeamPROP has immense functionality and is known for its wide flexibility and mode solving capabilities. Here I will be using it to perform relatively simple nonlinear simulations within bulk and waveguide objects, to study how a gaussian beam behaves in Cr:ZnSe under high powers.

Overview of simulations & launch parameters

Cr:ZnSe ULI waveguides have seen much success with being pumped at around 1.9 μm, as it is relatively close to the peak absorption wavelength (~ 1.75 μm) and there are a wide array of high power pump lasers at this wavelength. As seen from figure 24 it also has a high nonlinear refractive index than longer wavelengths and so will be useful for nonlinear applications. Here a pump wavelength of 1.908 μm will be assumed, as an IPG photonics Thulium-Fiber laser operating at this wavelength is available in the lab and has been previously used for mode locking. From the values shown in figure xx, this gives $n_2 = 1.411 \times 10^{-14}\, cm^2/W$.

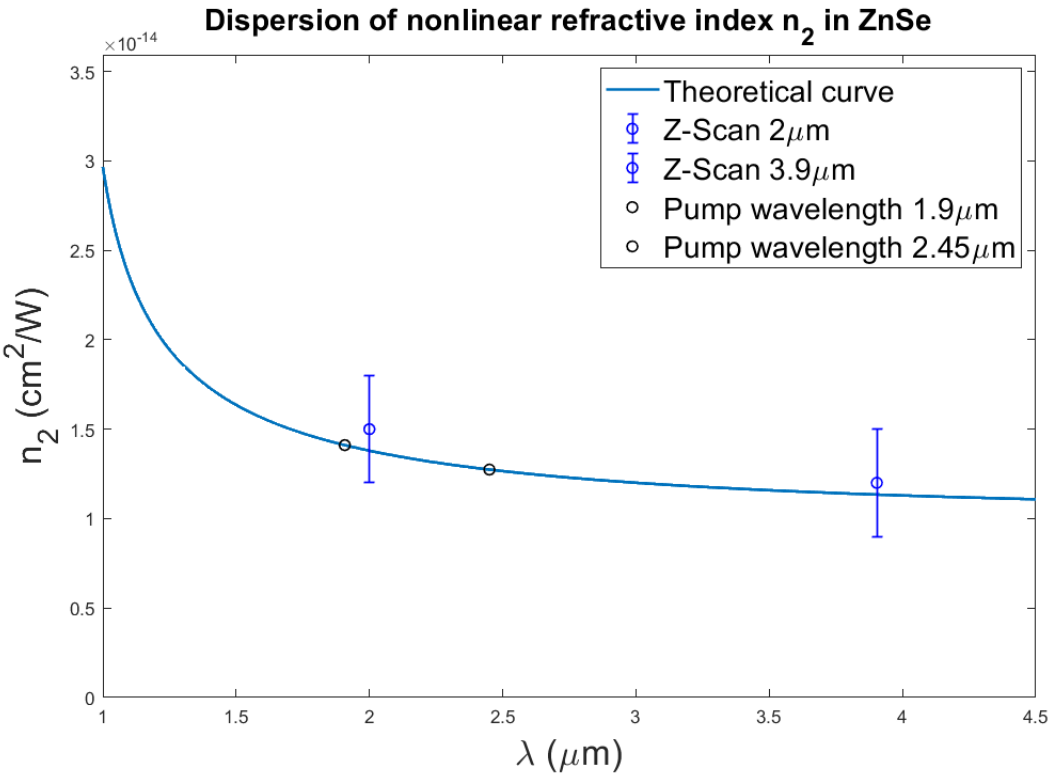

Figure 24: Wavelength dependence of the nonlinear refractive index in ZnSe (blue curve) found from the above analysis, along with two known experimental values. Also shown are values for the pump and lasing wavelength.

For self-focussing, there are three different cases that should be considered. The first is self-trapping, which is when the diffraction of the beam within the medium is balanced with this lensing effect which results in the beam width staying constant throughout. This occurs at a critical power

$$P_{cr} = \frac{\pi(0.61)^2\lambda_0^2}{8n_0n_2} \tag{2}$$

where λ_0 is the wavelength of the incident light, n_0 is the linear refractive index of the medium and n_2 being the intensity dependent refractive index.

Using the equation (2), along with linear and nonlinear refractive index values, the critical self-focusing power is calculated at 154.9 *kW*. This immediately shows the advantages of this material for nonlinear applications as the critical power for Ti:S is around 2.6 *MW* [59], almost 17 times smaller. BeamProp also requires the use of $\chi^{(3)}(\mu m^2/V^2)$ rather than n_2. This gives us a value 2.959×10^{-8} $(\mu m^2/V^2)$. One of the

most important launch parameters is the input beam type and dimensions. A gaussian beam will be used here to simulate a real pump laser, as mentioned this would be an IPG photonics Th:Fibre laser, which has a 1/e beam radius of 2 mm. Using equation (3) below, and a focal length of 10 cm, a suitable input radius of 30 μm can be calculated.

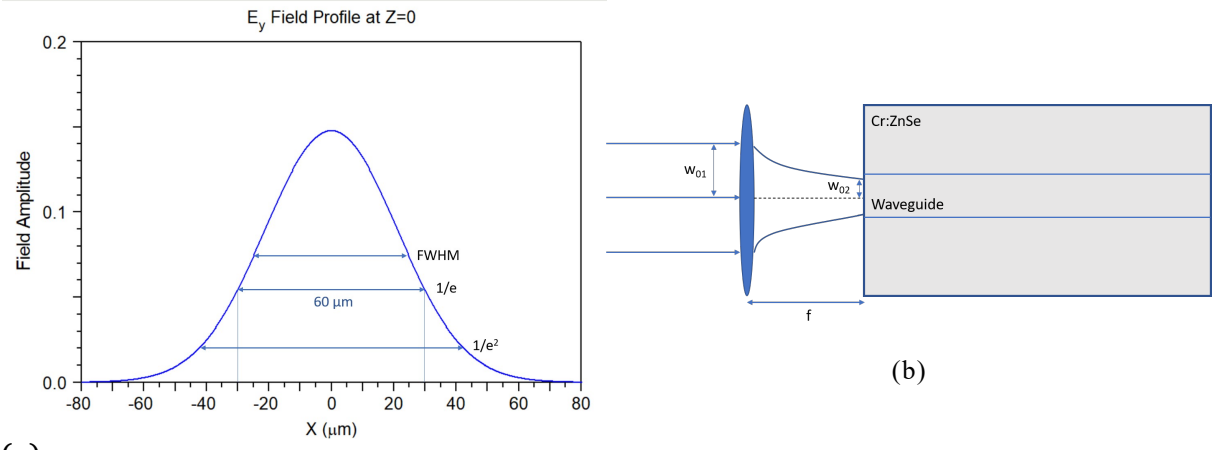

Figure 25: *a) Is a snapshot of the launch beam, with annotated width parameters, b) is a simplified schematic of how the light will be coupled into the waveguide from a gaussian beam of initial waist* w_{01}*, through a lens focal length f.*

$$w_{02} = \frac{f\lambda}{\pi w_{01} n_0} \tag{3}$$

It is also important to note that z_{sf} is the distance over which the beam becomes self-focused and is given by the following relation (for $P > P_{cr}$):

$$z_{sf} = w_0\sqrt{\frac{n_0}{2n_2 I}} = \frac{2n_0 w_0^2}{\lambda_0}\frac{1}{\sqrt{P/P_{cr}-1}} \tag{4}$$

Initially, self-trapping was tested within bulk Cr:ZnSe, in a basic 2D simulation. This was done by setting the background index to 2.434, i.e the same material as the medium we are testing. The assumption being made here is that there are no interactions with the boundary between the bulk medium and the surrounding air. This assumption can be further quantified, by measuring the amount of beam diffraction, and showing that the final diffracted beam width is too small to make it to the boundary of the medium. Additionally, there is no parameter in either equation

(2) or (4) to account for the surrounding medium. These simulations were performed for two different lengths, 1000 μm and 7000 μm. The former is to get a good idea of the effects that take place in the medium, and the latter is based on a typical Cr:ZnSe sample size 3x6x7mm [60]. To show that self-trapping occurs, it is necessary to compare it to the ordinary low power case when there are no nonlinear effects and the beam spreads due to diffraction within the material. Having shown self-trapping and understanding the parameters necessary to produce such a result, it was necessary to characterise self-focusing in bulk for various input powers.

The next step was to compare these results in bulk, to a channel waveguide geometry which is the focus of this project. By doing this we will be able to comment on the feasibility on using waveguides for nonlinear applications. There are two designs that were tested, the first being a standard continuous waveguide and the second being a coupled waveguide. The concept with the coupled waveguide is that the second waveguide would act as a hard aperture for Kerr-Lens mode locking, shown in the figure 26. A waveguide length of 7000 μm was used and the critical power for several waveguide diameters measured by varying the input power and looking at how the 1/e width changes. For the coupled waveguide, a length of 7000 μm was also used and the gap width varied to look at both output and critical powers.

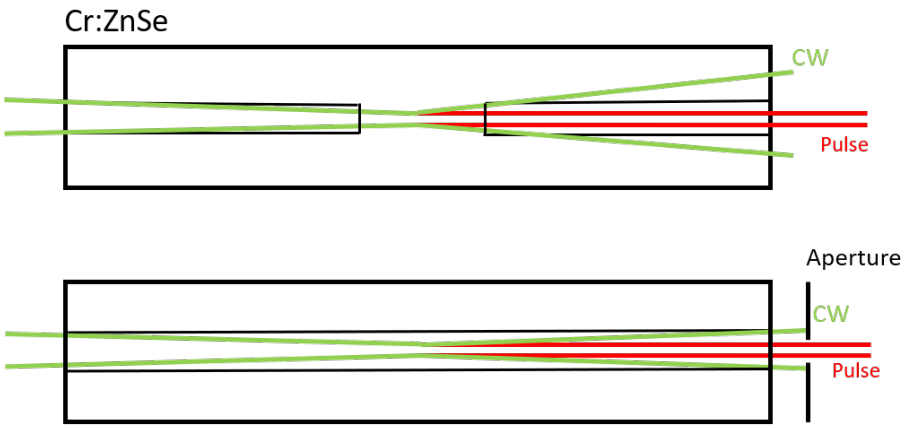

Figure 26: The two potential waveguide designs for KLM. The upper image shows a diagram of a coupled waveguide with the green CW mode being attenuated before fully propagating, and the red pulsed mode being favoured. The lower diagram demonstrates a standard waveguide design with an external aperture to induce KLM.

Diffraction and Self-trapping in Bulk

The critical power for self-focusing was previously found to be 154.9 kW, and the third order nonlinearity $\chi^{(3)} = 2.959 \times 10^{-8} \mu m^2/V^2$. There are several ways that RSoft can take this information as a launch parameter. The way that works best with in simulations with such high power is to keep the launch power constant at a value of 2 and vary the $\chi^{(3)}$ values so they are scaled in the following way:

$$P_0 = 2 \tag{5}$$

$$\chi(3) = P[W]\,\chi(3)[\mu m2/V\,2] \tag{6}$$

However, in 2D simulations these parameters were still too large and overloaded the simulation area. So I needed smaller values for the power that still correlated to our input. I tried various different approaches but I had success with dividing the critical power in kW by the 1/e width of the beam. This gave:

$$\frac{154.9 \times 10^3}{60} = 2581.7\ W/\mu m \tag{7}$$

We then used this input as the power modifier in front of the $\chi^{(3)}$ value and as seen in Figure 27 below, this showed self-trapping of the beam. This was my basis value that I used to compare others to.

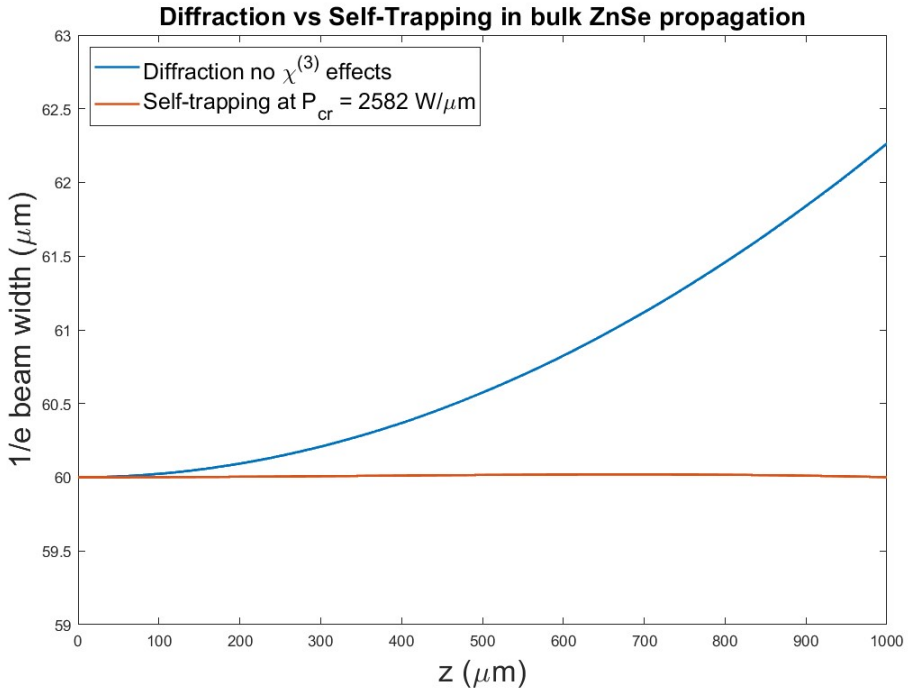

Figure 27: Diffraction and self-trapping in bulk ZnSe, a constant beam width throughout the sample shows self-trapping and the increase in beam width shows diffraction.

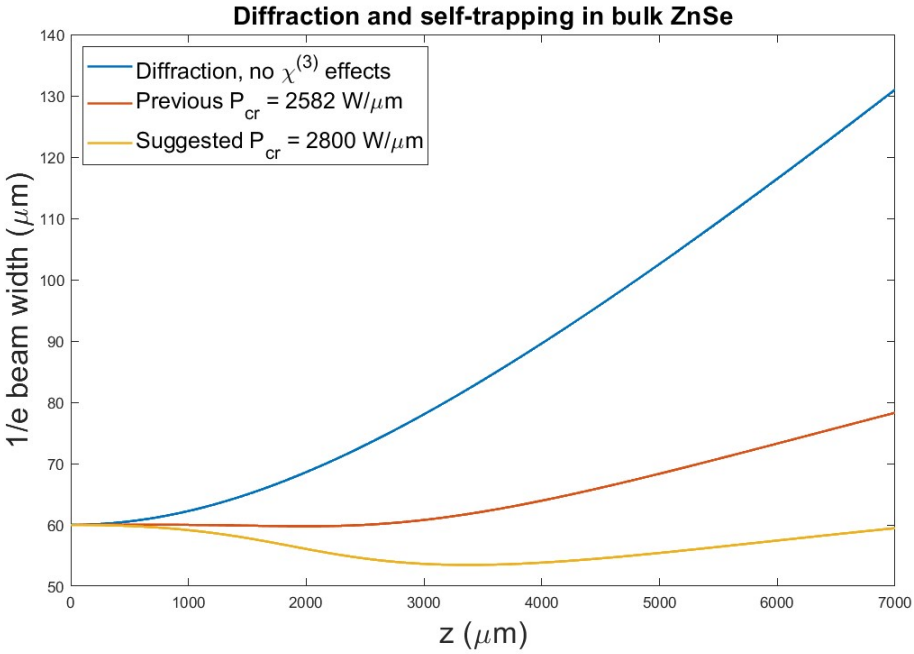

Figure 28: Diffraction and self-trapping for two different powers in bulk ZnSe. The orange curve is the behaviour of the beam using the critical power for the shorter length, and the yellow is for a higher power giving better self-trapping in the longer sample. Also shown is the diffraction within the material.

The above graphs show us that the amount of diffraction within a longer waveguide dramatically increases, overcoming the self-focusing seen in the shorter. This requires a higher amount of power, ~ 16%, to maintain a roughly constant beam diameter. To further test the critical power, we need to show that it correlates with the self focusing distance, given in equation (10). Using an arbitrary value of $2P_{cr}$, the beam width changes as shown below in figure 29.

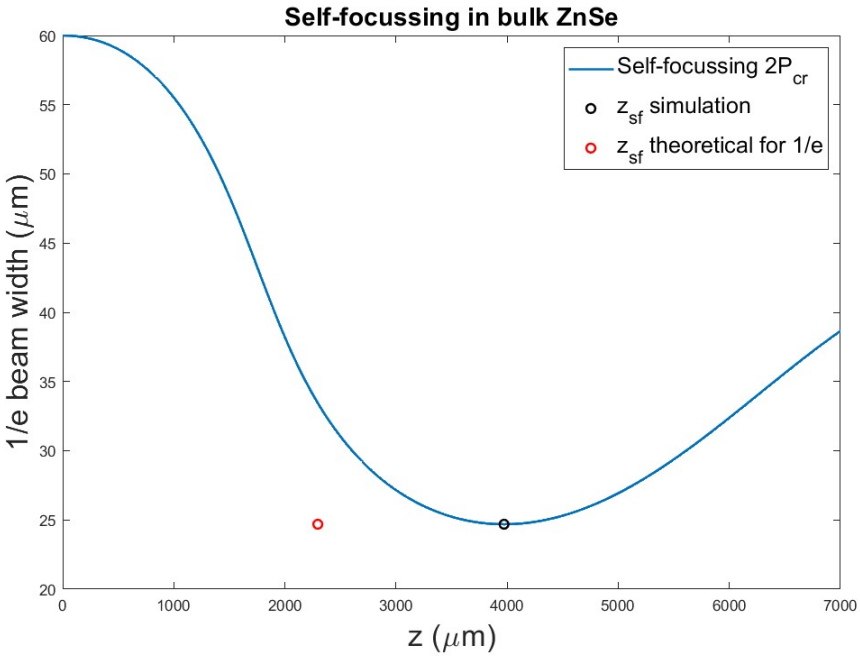

Figure 29: *A plot of beam width vs propagation distance in bulk. The minimum beam width at the 2Pcr self-focusing point is labelled (black) along with the theoretical value (red).*

The above figure shows how the beam becomes focused in the material due to the nonlinear refractive index. This is shown by a reduction in beam width by ~ 58%. This is a fundamental result as it gives an idea of the position of the focused beam within the material for a certain power. There is a fairly large percentage error between the simulated self-focused length (black circle), and the theoretically calculated value (red circle), of ~ 42%. There could be several reasons for this disparity. Equation (2) which is being used to calculate the theoretical distance is based on the situation where the beam is focused tightly to a spot, where the beam waist will be zero. The analysis done to produce this equation ignored effects of diffraction in the material and is just based

on Fermat's principle, hence why in reality the beam is not focused to an infinitesimal spot and there is an error in the self-focused distance.

Waveguide simulations

Continuous waveguides

To define a waveguide structure in BeamPROP, both a material and a background index is required. As a ULI structure is formed from an unchanged core and a reduced refractive index surrounding, I used the refractive index of ZnSe at the pump waveglength, 2.434, and a surrounding index of 2.433. Giving a difference of Δn = 0.001. The index profile along with the fundamental mode of an 80 μm diameter, 7000 μm long, 2D waveguide can be seen below.

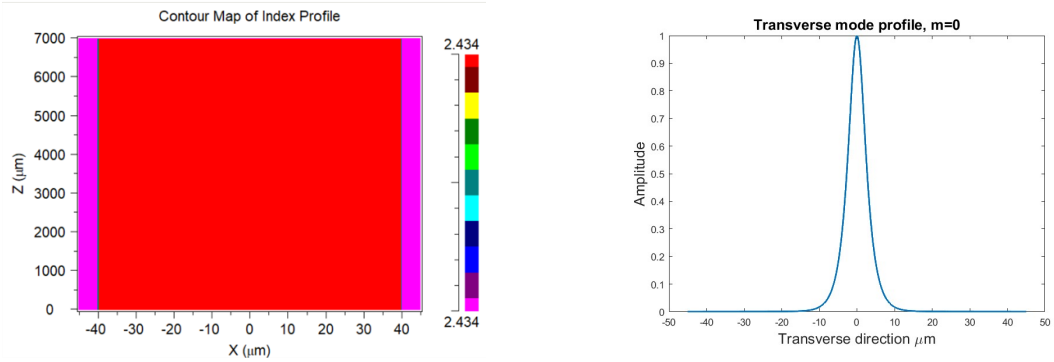

(a) (b)

Figure 30: a) Displays the refractive index profile, with a difference of 0.001, b) shows the fundamental mode of the waveguide.

The next stage was to calculate the critical power for a varying waveguide diameter, to see if they could be advantageous in this aspect. I started with a relatively large waveguide, 100 μm, and tested it with the critical power for bulk. I then looked for the point where the input beam width stayed constant throughout, and took several readings for the launch power at the point I believed this was. The diffraction and self-trapping in a waveguide is shown below.

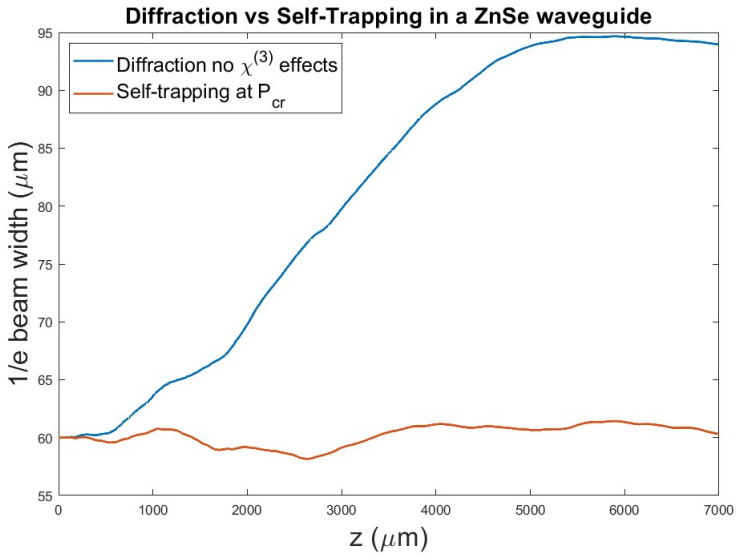

Figure 31: Diffraction and self-trapping plots of the beam width propragation through a waveguide. Diffraction is shown by the blue curve and self-trapping by the orange.

It can be seen that the self-trapping and diffraction are not as smooth as in bulk, due to the boundary interactions that take place within the waveguide. I measured the critical power for self-trapping in six different diameter waveguides, ranging from 75 – 100 μm.

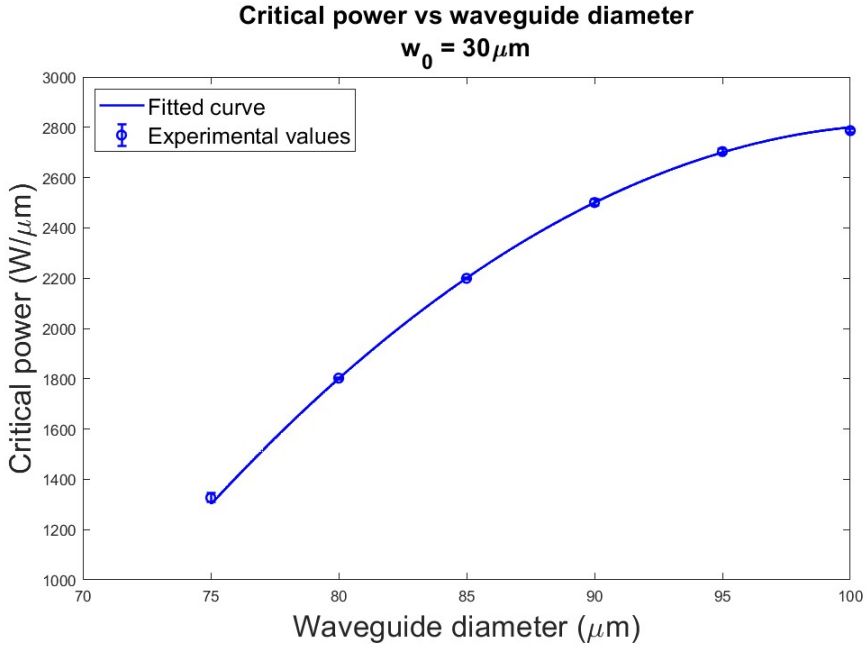

Figure 32: *Plotted values of the critical power for varying waveguide diameters. Errors plotted are calculated as standard error from repeat measurements.*

The above results show a trend for decreasing self-trapping critical power, as the waveguide diameter is reduced by a constant amount. For the largest tested waveguide it can be seen that the critical power tends towards that of bulk (2800 $W/\mu m^2$), but for the smallest of the waveguides, it has been reduced by at least 50%. For waveguides below $75\mu m$ it was not possible to tell where the critical power occurred as there was an increased level of interactions with the more confined boundaries of the waveguide, meaning that the beam propagated with more or less a constant width regardless of the nonlinear effects.

Once the critical power for self-trapping within waveguides was probed, the next stage involved higher powers for self-focusing. Self-focusing was previously seen in bulk (figure 29) at two times the critical power. In order to acquire a broader look into the self-focusing at more than just one power, it was varied from 1.5-5 times the critical power and the minimum beam width values and the distances at which they occurred were extracted. These values were then plotted against each other to form an idea of the strength of self-focusing at different distances within the material. This process was then repeated with an $80\mu m$ waveguide and the results were similarly plotted. As the critical power in a waveguide is less, consequently the value of 5 times the critical power is going to be less than in bulk. Therefore some higher power values for the waveguide were added to match the bulk and make sure that similar powers could be examined in each.

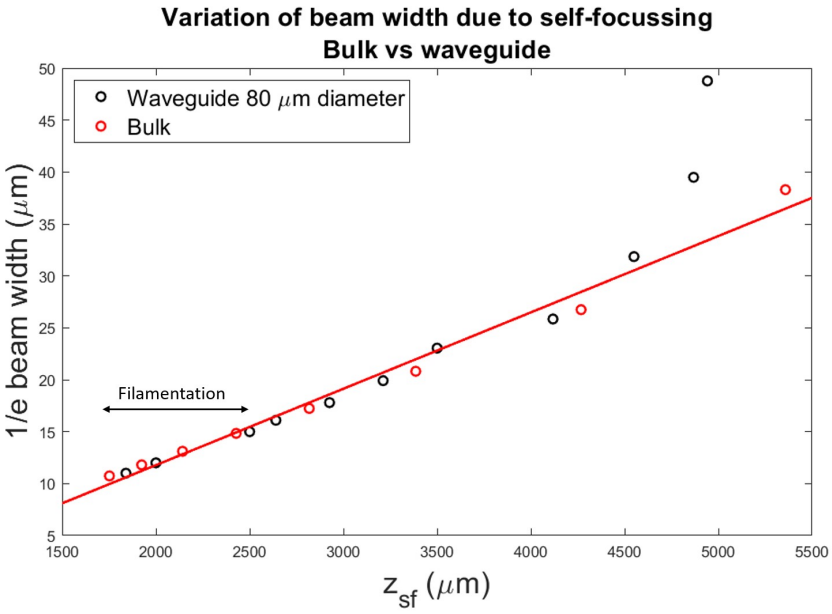

Figure 33: Minimum values for the beam width at self-focused points for both bulk (red) and waveguide (black). Red line is the straight line fit for the bulk values.

There are several noteworthy things to discuss about the above plot of beam width vs z_{sf}. The first being that in a bulk material, the beam width can be assigned well with a straight line fit, whereas in a waveguide it diverges for lower powers. This could be due to generally lower powers in the system meaning the beam is not as tightly focused within the material. This is supported by the fact that for higher powers ($\geq 2.5P_{cr}$) the linear fit for the bulk results also corresponds well with the waveguide results. These results show that similar levels of self-focusing occur in both bulk and waveguide geometries.

However, at higher powers filamentation becomes a problem. This is where the beam is broken up into filaments due to constant focusing, diffraction and re-focusing within the material. This can become a problem, leading to damage of the medium. Filamentation becomes a significant at powers of $3.5P_{cr}$ in bulk and $5.5P_{cr}$ in an 80 μm waveguide. I have annotated this range on the above plot. These values plotted are only for the first point of self-focusing, the second point has not been included here for simplicity.

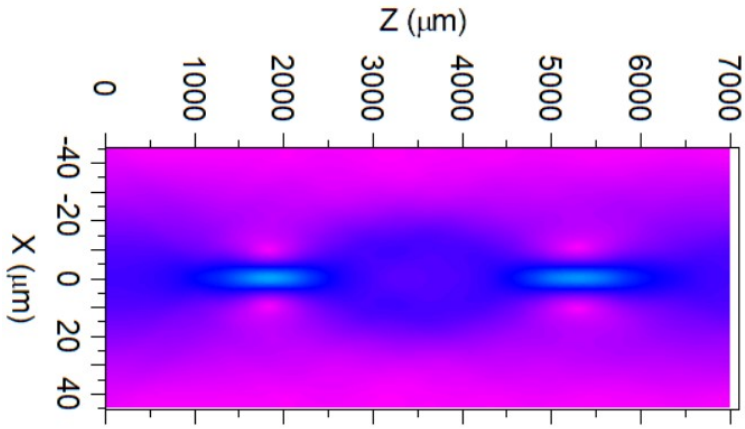

Figure 34: Contour map of field amplitude showing filamentation within a waveguide, the beam is self-focused at several points along the length of the waveguide (light blue points) Coupled waveguides

Coupled Waveguides

To simulate the coupled waveguides discussed earlier, i.e. two inscribed lines forming the waveguide are needed, with a gap of un-irradiated core material. The index profile of such a structure using BeamPROP can be seen in figure 21. The aim of the following analysis is to determine whether a coupled waveguide like this could be used for continuous wave lasing and then KLM.

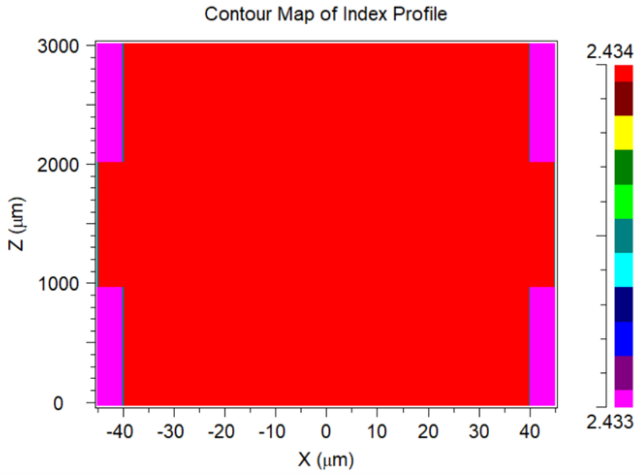

Figure 35: Refractive index profile of coupled waveguide, the pink regions represent the inscribed refractive index change, the red representing the unchanged core material.

To characterise this coupled waveguide, I started by viewing the output power of a Cr:ZnSe waveguide without the gap. The waveguide diameter was chosen to be 80 μm which has a corresponding critical power of 1800 $W/\mu m$. The gap width was then increased in length from 500 – 5000μm and the total power throughout the waveguide and the final output power were examined. This was done for low powers with no self-focusing present to get a general idea of how such a design would operate.

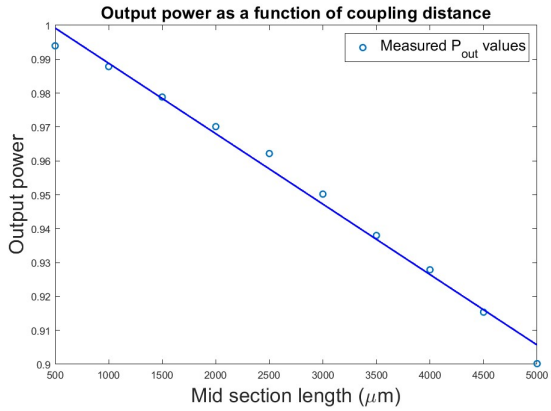

Figure 36: *Power characterisation of coupled waveguides. The figure shows the singular output powers from the coupled waveguide and the relevant straight line fit for different gap widths.*

The results show that the output power decreases as the length of the gap is increased, as expected. However, for the largest of the gaps (5000μm) this is only a difference of ~ 10%. This shows that the coupling between the two waveguides is fairly efficient and could potentially be used for lasing. The next stage is to deduce how the coupled waveguides act under higher intensity light, i.e. with nonlinear effects. I chose to look at just the critical power again for a range of gap widths from 500 – 5000μm. These results are shown below.

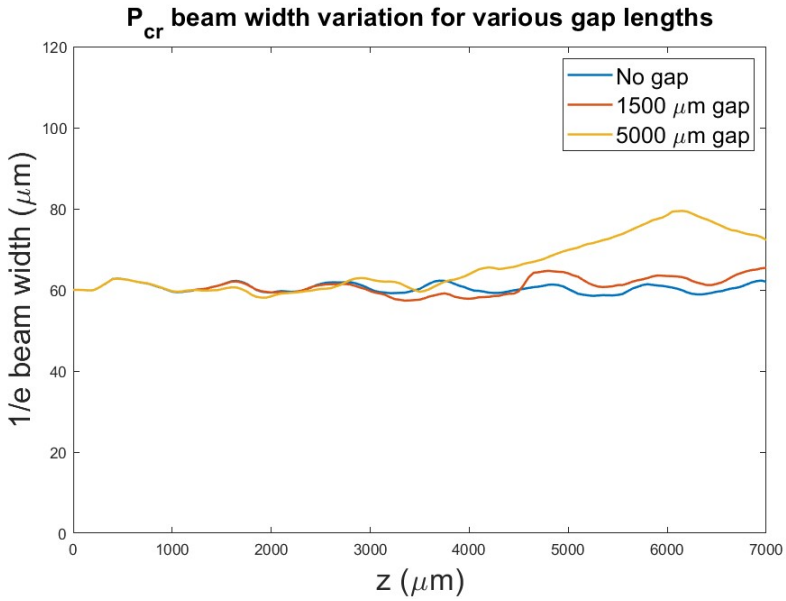

Figure 37: Plot of beam width throughout coupled waveguide for various different gap lengths. All configurations using the same critical power as that for the regular waveguide

It can be seen that for longer gap length, the beam diverges away from its self-trapping width due to the additional diffraction that becomes significant in the bulk portion of the waveguide. I found that for gaps greater than 1500 μm the beam stopped being self-trapped and would require higher powers. So a preliminary inquiry has been undergone into the effectiveness of the coupled waveguide geometry, which was the second idea for how to Kerr-lens mode-lock a waveguide laser. Initial results show that a relatively small coupled gap would not induce a large loss and hence could potentially be used.

Discussion

Discussion of results

The multi-stage process leading up to the simulation outcomes are described, involved understanding nonlinear optics theory, using this to gather relevant parameters and finally using software to visualise these effects in three different material geometries. The first being bulk, the second a standard waveguide and the third a coupled waveguide. The motivation behind this was to try and understand whether these objects could be used in the field of Kerr-Lens mode locking.

The most promising results come from the continuous waveguide, where results of self-trapping and self-focusing are discussed in continuous waveguides. These results show that the initial starting of the KLM process could be easier due to the lower critical powers required for self-trapping. By lowering this criterion, a smaller noise spike would be needed to induce this process, which could be beneficial as the error of misaligning the laser could be reduced. Additionally, smaller powers are needed in the system, lowering the chance of material damage and easing the specifications on what pump lasers can be utilised. The results shown in figure 19 show that similar levels of self- focusing occurs both in bulk and waveguide. This is encouraging as it shows the favourable properties of bulk are not lost when transitioning to a waveguide, while reducing on the critical power.

For the coupled waveguide simulations, a linear decrease in power was demonstrated as the width of the gap increased by constant increments. This loss had a maximum of ~ 10% for a gap of 5000 μm. The critical power for self-trapping in the continuous waveguide, worked relatively well up to a gap width of ~ 1500 μm for the coupled waveguide. So, a waveguide gap this length would only induce a loss of ~ 2% meanwhile maintaining a critical power of that seen in a regular waveguide. This would be a good place to start if such a device were to be tested in the lab. However, there are several reasons practically that a coupled waveguide would not work for KLM purposes. The first being that prior to KLM, the device needs to be able to lase well in CW. Despite the results showing that losses are relatively low, in reality these may be too large to sustain lasing.

There are several limitations to the method and analysis that has been carried out here, which have been placed into several categories. The first category being understanding of the physics. In all simulations undertaken here, the pump wavelength (1.9 μm) has been used as the input wavelength for all devices. However, in KLM, the self-focusing effects that take place are induced once the device is already lasing in CW. Therefore, in reality the process will be started by the lasing wavelength (~ 2.4μm) rather than the pump. This isn't a detrimental issue as looking at values of n_2 and n_0 for the two different wavelengths, the variation is very small and hence is unlikely to have a significant impact on the results. However, it demonstrates a misunderstanding of the theory and needs to be noted. The second category, is simulation parameters and use

of the software. Throughout the simulations a beam diameter of 60 μm was used, justified in 3.2 with the use of a 10 cm focal lens and the properties of a specific pump laser. However, this focal length is fairly arbitrary, used mainly in focusing the beam for the purposes of CW lasing[44]. In practice this focal length is widely different and is of the upmost importance in finding regions at which KLM can be sustained. In hindsight and with more time permitted, I should have taken results for a range of different input beam diameters, corresponding to focal lengths of known KLM regions for the cavity that was decided on. Additionally, only one length of waveguide was used, corresponding to a standard size that has been used before in [60] for mode locking with a SESAM. However, from the bulk investigation, it was shown that higher powers are needed for self-trapping. A shorter waveguide would therefore be more ideal for KLM which is also supported in literature[49], hence additional simulations should be done in order to determine suitable lengths. The third is material properties. The principle aim of this project was to focus in on Cr^{2+} doped Zinc Selenide in particular, however only the optical properties for undoped ZnSe have been used. It is unclear in the literature how the doping affects such properties so here the assumption is that it is negligible. Obviously in practice this is untrue however I believe that like the pump and lasing wavelength issue discussed, the difference in values would be insignificant.

Future work

As discussed, there were several limitations to the simulation work so therefore prior to taking this idea into the lab some additional results should be taken for different length waveguides, different input beam diameters and for the lasing wavelength rather than the pump wavelength. The next stage for this project would be to fabricate various waveguides in Cr:ZnSe and attempt KLM. These waveguides would be fabricated using ULI, a benefit of this technique being that both the continuous waveguide and coupled waveguide could be built into one bulk sample, and then tested individually. I would start by fabricating and characterising an 80 μm diameter depressed cladding waveguide in continuous wave mode in a compact three-element cavity. This diameter is chosen as it has been used for mode locking with a SESAM[27] due to its favourable qualities. After this, stability regions where KLM can be supported in this set can be found in ref.[49] and Kerr-Lens mode locking can be attempted.

Within the Cr:ZnSe bulk substrate, several coupled waveguides could easily be written with varying gap widths up to 1500 μm and potentially beyond this. Therefore, the smallest gap could be tested for CW lasing and if successful the gap could be increased until it became unsustainable. Then the same three element cavity could be used to test KLM without a hard aperture, attempting to use the coupled geometry instead.

Conclusion

In conclusion, this project report details various different methods for researching nonlinear properties of bulk and waveguides in Cr:ZnSe specific to Kerr-Lens mode locking. Starting from the theory of effects arising from the third order nonlinearity, this knowledge was then used to find important values such as nonlinear refractive index n_2 and the critical power for self-trapping P_{cr}. In order to obtain results that may give a further understanding into these effects, the software BeamPROP was used to model the propagation of light in both bulk, waveguide and coupled waveguide devices. It was found that waveguides possess lower critical powers and levels of self focusing close to that of bulk, establishing that they could be promising candidates for Kerr-Lens mode locking. In addition to this, the output and critical power in coupled waveguides was also investigated. As well as the theoretical and experimental results obtained, relevant background theory into ultrafast laser inscription, its applications in Cr:ZnSe and Kerr-lens mode locking was looked at in detail. This allowed for the suggestion of a compact three element cavity to be used in conjunction with the waveguides for initial testing of continuous wave and KLM if further practical work was to be carried out on this project in the future.

Direct Comparison of KLM Bulk and HIP Cr:ZnSe

Introduction

The outstanding research carried out in AFRL in the development of HIP samples opened up the potential of achieving bandwidth limited pulses in homogeneously broadened Cr:ZnSe system. To quantify the role of homogeneous broadening, it is very appropriate to investigate the Kerr-Lens Mode Locking on the same piece of Cr:ZnSe before and after the HIP treatment. In addition, we are also investigating the role of pump wavelength e.g. Tm:Fiber (1.9 μm) and Er:Fiber (1.57 μm).

Bulk Cr:ZnSe

Laser resonator and experimental results for CW laser action.

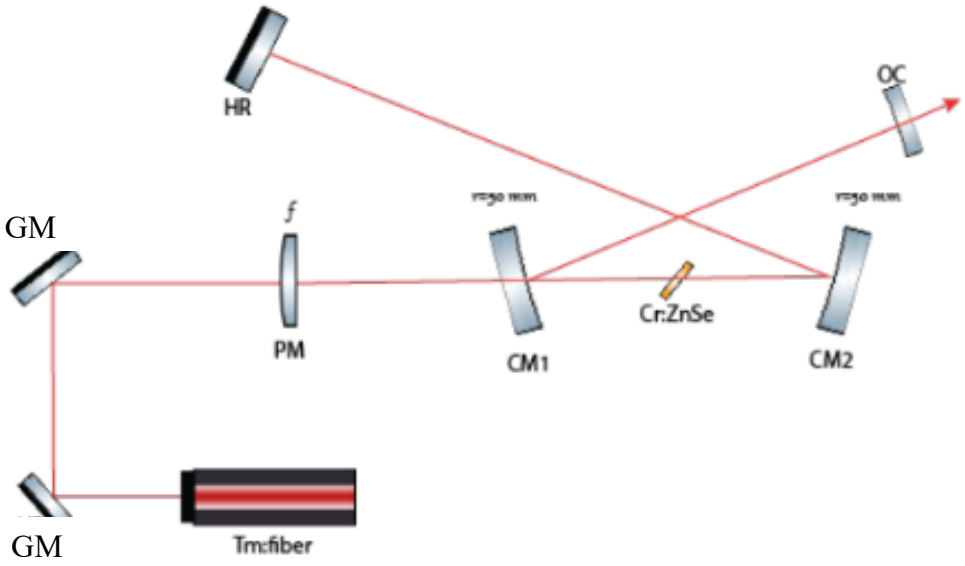

Figure 38: Laser resonator for CW laser experiment. PM: plano-covex lens 50 mm focal length; CM: curved chirped mirror (50-mm radius of curvature); HR: plane chirped mirror; GM: gold mirror; OC: output coupler (1%, 3%, and 20%). The arm lengths were arranged in accordance with near 1:1 ratio (in particular, the lengths were adjusted to about 300 mm).

The calculated spot sizes in the laser crystal are: 31 – 35 μm for the pump radiation (at 1.94 μm) and 30 - 32 μm for the laser wavelength (at 2.45 μm).

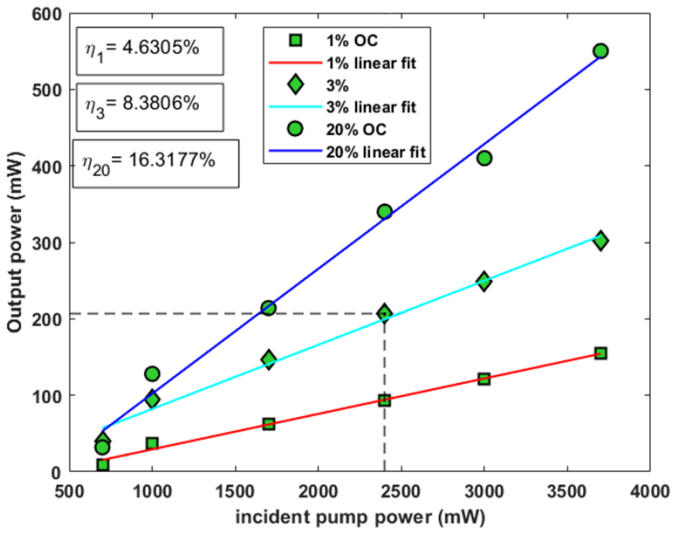

Figure 39: Input output characteristics for Tm:fiber pumping.

Laser resonator and experimental results for Kerr-lens mode locking laser action.

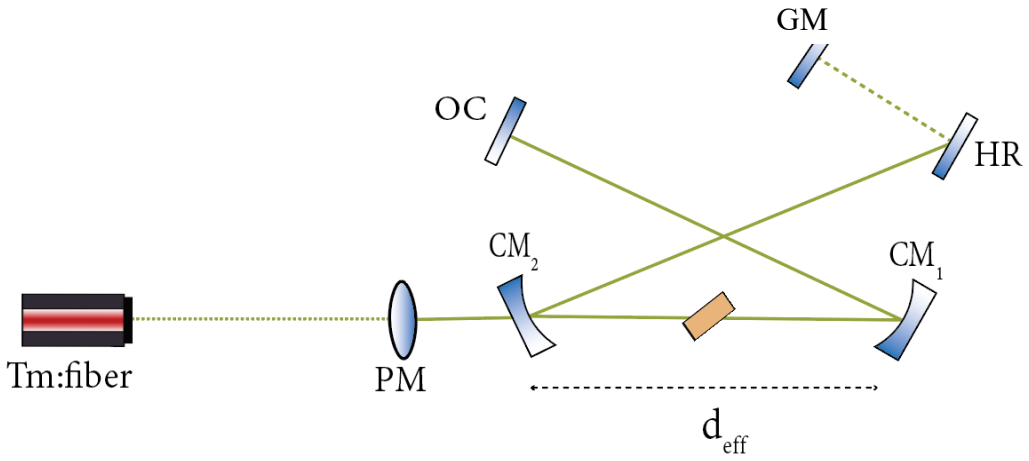

Figure 40: Laser resonator for CW laser experiment. PM: plano-covex lens 40 mm focal length; CM: curved chirped mirror (50-mm radius of curvature); HR: plane chirped mirror; GM: gold mirror; OC: output coupler (1%, 3%, and 20%). The arm lengths were arranged in accordance with 5:3 ratio (in particular, the lengths were adjusted to 665 mm and 297 mm respectively). The deff separation between the CM was in the II stability region from 51.7 mm to 52.2 mm.

The spot sizes in the laser crystal are: 25 – 29 μm for the Tm:fiber laser pump radiation (at 1.94 μm); 18 – 21 μm for the Er:fiber laser pump radiation (at 1.57 μm) and spot size w_o = 25 – 28 μm for the laser wavelength.

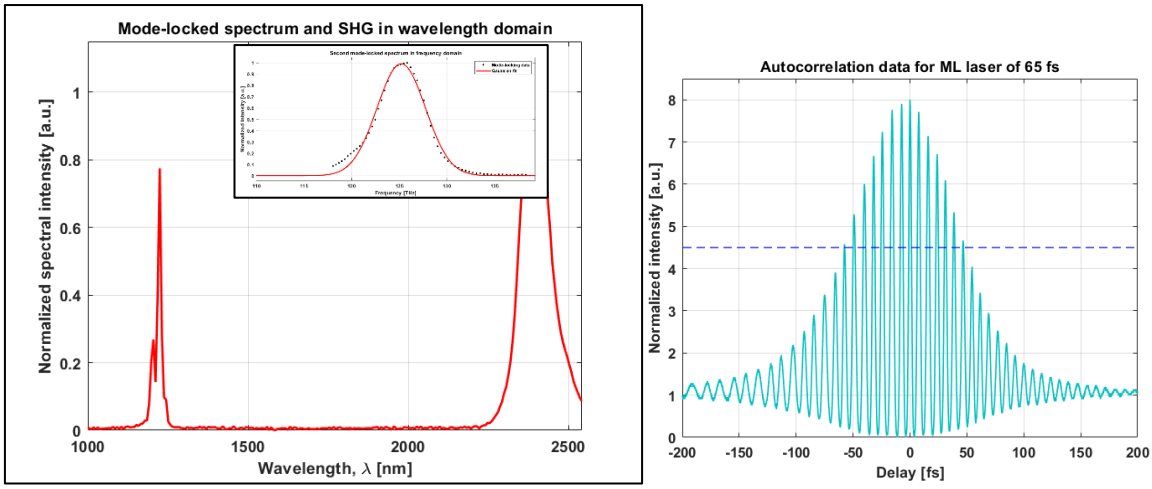

Figure 41: Pulse spectrum and autocorrelation trace in Kerr-lens mode-locking using Tm:fiber laser pump (3.7 W pump power, 150 mW average output power, 150 MHz repetition rate). The threshold pump power for mode-locking action is 2.4 W (with an average output power of 97 mW)

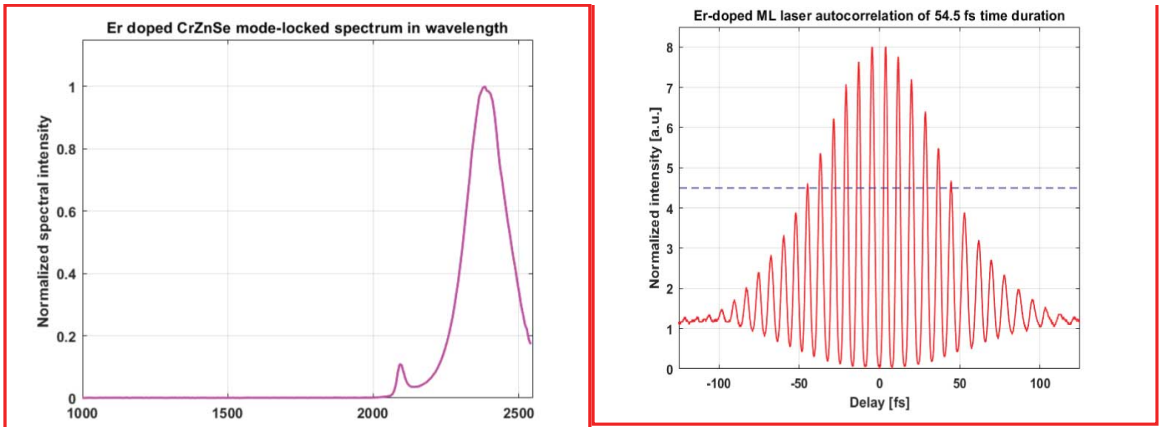

Figure 42. Pulse spectrum and autocorrelation trace in Kerr-lens mode-locking using Er:fiber laser pump (3 W pump power, 60 mW average output power, 150 MHz repetition rate).

Discussion

This bulk sample is now HIP treated. The experiments are being undertaken now to investigate the Kerr-Lens mode locking in this HIP sample. This will for the first time will give us an insight into the role of HIP treatment in the generation of few-cycle laser pulse in mid-infrared region by using Cr:ZnSe as a gain medium.

Publications and Forthcoming Publications

Title	Lead Author/Presenter & Description	Journal/Conference
Mid-IR Ultrafast Laser Inscribed Waveguides and Devices	Sean McDaniel Review of advances in the creation of guided wave devices in Mid-IR compatible media.	2019 IEEE Research and Applications of Photonics in Defence Conference (RAPID). Miramar Beach, Florida, USA
Cr:ZnSe Laser – CW and Ultrashort Pulses	Ajoy Kar	2020 IEEE Research and Applications of Photonics in Defense Conference (RAPID). USA Virtual Conference.
Chalcogenide Photonics	Ajoy Kar	2020 Recent Advances in Materials Science and Engineering (RAMSE) RAMSE-2020. India Virtual Conference.
A bright source of telecom single photons based on quantum frequency conversion	Fiona Thorburn and Ajoy Kar The application of tuneable Cr:ZnSe laser	Applied Physics Letters, **118**, 17, 174003, 2021.
Integrated Photonic Manufacturing Enabled by Ultrafast Laser Technology	Ajoy Kar	2021 1st International Conference on Advances in Materials Science (ICAMS-2021). India Virtual Conference.
Integrated Photonic Manufacturing Enabled by Ultrafast Laser Technology	Ajoy Kar	2021 Frontiers in Optics & Photonics 2021(FOP21). India. Virtual Conference.
Ultrafast hot-isostatic pressed Cr:ZnSe Laser at 2.4 μm	Fiona Thorburn Report of sub 40 fs ultrafast HIP treated Cr:ZnSe laser	Under preparation.
The role of HIP treatment in the generation of few-cycle laser pulse in mid-infrared region by using Cr:ZnSe as a gain medium.	Experiment in Progress	Experiment in progress
Mid-IR Waveguide Lasers in Transition Metal Doped II-VI Semiconductors	Adam Lancaster	PhD Thesis

Compact High Repetition Rate Mid-infrared Solid-state Lasers	Fiona Thorburn	PhD Thesis

References

1. B. M. Walsh, H. R. Lee, and N. P. Barnes, "Mid infrared lasers for remote sensing applications," Journal of Luminescence **169**, 400-405 (2016).
2. A. P. Patel and B. E. Knudsen, "Optimizing use of the holmium:YAG laser for surgical managment of urinary lithiasis," Current Urology Reports **15**, 397 (2014).
3. A. Sijan, "Develpment of military lasers for optical countermeasuers in the mid-IR," in *SPIE Security + Defence*, 2009), 748304.
4. A. H. Nejadmalayeri, P. R. Herman, J. Burghoff, M. Will, S. Nolte, and A. Tünnermann, "Inscription of optical waveguides in crystalline silicon by mid-infrared femtosecond laser pulses," Optics Letters **30**, 964-966 (2005).
5. U. Keller, "Recent developments in compact ultrafast lasers," Nature **424**, 831-838 (2003).
6. S. Vasilyev, I. Moskalev, M. Mirov, V. Smolski, S. Mirov, and V. Gapontsev, "Kerr-Lens Mode-Locked Middle IR Polycrystalline Cr:ZnS Laser with a Repetition Rate 1.2 GHz," in *Lasers Congress 2016 (ASSL, LSC, LAC)*, OSA Technical Digest (online) (Optical Society of America, 2016), AW1A.2.
7. D. A. Braje, M. S. Kirchner, S. Osterman, T. Fortier, and S. A. Diddams, "Astronomical spectrograph calibration with broad-spectrum frequency combs," The European Physical Journal D **48**, 57-66 (2008).
8. E. Sorokin, I. T. Sorokina, M. S. Mirov, V. V. Federov, I. S. Moskalev, and S. B. Mirov, "Ultrabroad Continuous-Wave Tuning of Ceramic Cr:ZnSe and Cr:ZnS Lasers," in *Advanced Solid-State Photonics* (San Diego, 2010).
9. I. Moskalev, S. Mirov, M. Mirov, S. Vasilyev, V. Smolski, Z. A, and V. Gapontsev, "140 W Cr:ZnSe laser system," Optics Express **24**, 21090-21104 (2016).
10. L. D. DeLoach, R. H. Page, G. D. Wilke, S. A. Payne, and W. F. Krupke, "Transition Metal-Doped Zinc Chalcognides: Spectroscopy and Laser Demonstration of a New Class of Gain Media," IEEE Journal of Quantum Electronics **23**, 885-895 (1996).
11. M. Ebrahimzadeh, "Mid-Infrared Ultrafast and Continuous-Wave Optical Parametric Osciallators," in *Solid-State Mid-Infrared Laser Sources, Topics in Applied Physics*, I. T. Sorokina and K. L. Vodopyanov, eds. (Springer-Verlang, Berlin Heidelberg 2003).

12. Y. Bai, S. Slivken, S. Kuboya, S. R. Darvish, and M. Razeghi, "Quantum cascade lasers that emit more light than heat," Nature Photonics **4**, 99-102 (2010).
13. Y. Bai, N. Bandyopadhyay, S. Tsao, S. Slivken, and M. Razeghi, "Room temperature quantum cascade lasers with 27% wall plug efficiency," Applied Physics Letters **98**, 181102 (2011).
14. S. Mirov, I. Moskalev, S. Vasilyev, V. Smolski, V. Federov, D. Martyshkin, J. Peppers, M. Mirov, A. Dergachev, and V. Gapontsev, "Frontiers of mid-IR lasers based on transition metal doped chalcogenides," IEEE Journal of Selected Topics in Quantum Electronics, 08295223 (2018).
15. K. Petermann, "Oxide laser crystals doped with rare earth and transition metal ions," in *Handbook of solid-sate lasers*, B. Denker and E. Shklovsky, eds. (Woodhead Publishing, 2013), pp. 3-27.
16. W. R. Rapoport and C. P. Khattak, "Titanium sapphire laser characteristics," Applied Optics **27**, 2677-2684 (1988).
17. J. Peppers, V. V. Fedorov, and S. B. Mirov, "Mid-IR photoluminescence of Fe2+ and Cr2+ ions in ZnSe crystal under excitation in charge transfer bands," Optics Express **23**, 4406-4414 (2015).
18. H. A. Jahn, E. Teller, and G. F. Donnan, "Stability of polyatomic molecules in degenerate electronic states - I—Orbital degeneracy," Proceedings of the Royal Society of London. Series A - Mathematical and Physical Sciences **161**, 220-235 (1937).
19. M. Kaminska, J. M. Baranowski, S. M. Uba, and J. T. Vallin, "Absorption and luminescence of Cr2+(d4) in II-VI compounds," Journal of Physics C: Solid State Physics **12**, 2197-2214 (1979).
20. C. E. Housecroft and A. G. Sharpe, "*d*-Block chemistry: coordination complexes," in *Inorganic Chemistry Second Edition,* 2nd ed. (Pearson Education Limited, 2005).
21. S. B. Mirov, V. V. Fedorov, D. Martyshkin, I. S. Moskalev, M. Mirov, and S. Vasilyev, "Progress in Mid-IR Lasers Based on Cr and Fe-Doped II–VI Chalcogenides," IEEE Journal of Selected Topics in Quantum Electronics **21**, 292-310 (2015).
22. S. Vasilyev, I. Moskalev, M. Mirov, V. Smolski, S. Mirov, and V. Gapontsev, "Recent Breakthroughs in Solid-State Mid-IR Laser Technology," Laser Technik Journal **13**, 24-27 (2016).

23. T. J. Carrig, G. J. Wagner, A. Sennaroglu, J. Y. Jeong, and C. R. Pollock, "Mode-locked Cr^{2+}ZnSe laser," Optics Letters **25**, 168-170 (2000).
24. C. R. Pollock, N. A. Brilliant, D. Gwin, T. J. Carrig, W. J. Alford, J. B. Heroux, W. I. Wang, I. Vurgaftman, and J. R. Meyer, "Mode locked and Q-switched Cr:ZnSe laser using a Semiconductor Saturable Absorbing Mirror (SESAM)," in *Advanced Solid-State Photonics*, Technical Digest (Optical Society of America, 2005), TuA6.
25. I. T. Sorokina and E. Sorokin, "Femtosecond pulse generation from a SESAM mode-locked Cr:ZnSe laser," Conference on Lasers and Electro-Optics/Quantum Electronics and Laser Science Conference and Photonic Applications Systems Technologies, Technical Digest (CD) (Optical Society of America, 2006), paper CMQ2. (2006).
26. I. T. Sorokina and E. Sorokin, "Chirped-mirror dispersion controlled femtosecond Cr:ZnSe laser," in *Advanced Solid-State Photonics, OSA Technical Digest Series (CD) (Optical Society of America, 2007), paper WA7.*, (2007).
27. E. Sorokin and I. T. Sorokina, "Ultrashort-pulsed Kerr-lens modelocked Cr:ZnSe laser," in *CLEO/Europe and EQEC 2009 Conference Digest*, (Optical Society of America, 2009), CF1_3.
28. M. N. Cizmeciyan, J. W. Kim, S. Bae, B. H. Hong, F. Rotermund, and A. Sennaroglu, "Graphene mode-locked femtosecond Cr:ZnSe laser at 2500 nm," Optics Letters **38**, 341-343 (2013).
29. J. Ma, G. Xie, P. Lv, W. Gao, P. Yuan, L. Qian, U. Griebner, V. Petrov, H. Yu, H. Zhang, and J. Wang, "Wavelength-versatile graphene-gold film saturable absorber mirror for ultra-broadband mode-locking of bulk lasers," Scientific reports **4**, 5016-5016 (2014).
30. S. Vasilyev, M. Mirov, and V. Gapontsev, "High Power Kerr-Lens Mode-Locked Femtosecond mid-IR Laser with Efficient Second Harmonic Generation in Polycrystalline Cr2+:ZnS and Cr2+:ZnSe," in *Advanced Solid State Lasers*, OSA Technical Digest (online) (Optical Society of America, 2014), AM3A.3.
31. Y. Wang, T. T. Fernandez, N. Cocuccelli, A. Gambetta, P. Laporta, and G. Galzerano, "47-fs Kerr-lens mode-locked Cr:ZnSe laser with high spectral purity," Optics Express **25**, 25193-25200 (2017).

32. N. Nagl, S. Gröbmeyer, V. Pervak, F. Krausz, O. Pronin, and K. F. Mak, "Directly diode-pumped, Kerr-lens mode-locked, few-cycle Cr:ZnSe oscillator," Optics Express **27**, 24445-24454 (2019).
33. A. Lancaster, "Mid-IR Waveguide Lasers in Transition Metal Doped II-VI Semiconductors " (Heriot Watt University Edinburgh, 2017).
34. S. McDaniel, A. Lancaster, R. Stites, F. Thorburn, A. Kar, and G. Cook, *Cr:ZnSe guided wave lasers and materials*, SPIE LASE (SPIE, 2017), Vol. 10082.
35. R. W. Sites, S. A. McDaniel, J. O. Barnes, D. M. Krein, J. H. Goldsmith, S. Guha, and G. Cook, "Hot isostatic pressing of transition metal ions into chalcogenide laser host crystals," Optical Material Express **6**, 3339-3353 (2016).
36. H. V. Atkinson and S. Davies, "Fundamental aspects of hot isostatic pressing: An overview," Metallurgical and Materials Transactions A **31**, 2981-3000 (2000).
37. J. Sanghera, W. Kim, G. Villalobos, B. Shaw, C. Baker, J. Frantz, B. Sadowski, and I. Aggarwal, "Ceramic Laser Materials," Materials (Basel) **5**, 258-277 (2012).
38. H. Namba, H. Osaka, K. Kamon, and F. Higuchi, "Process for preparing ZnSe single crystal," 4,584,053 (1986).
39. M. Chen, H. Cui, W. Li, H. Kou, J. Li, Y. Pan, and B. Jiang, "Reparative effect of diffusion process on host defects in Cr2+ doped ZnS/ZnSe," Journal of Alloys and Compounds **597**, 124-128 (2014).
40. J. W. Evans, R. W. Stites, and T. R. Harris, "Increasing the performance of an Fe:ZnSe laser using a hot isostatic press," Opt. Mater. Express **7**, 4296-4303 (2017).
41. J. R. Macdonald, S. J. Beecher, P. A. Berry, G. Brown, K. L. Schelper, and A. K. Kar, "Efficient mid-infrared Cr:ZnSe channel waveguide laser operating at 2486 nm," Optics Letters **38**, 2194-2196 (2013).
42. S. A. McDaniel, "MID-IR ULTRAFAST LASER INSCRIBED WAVEGUIDES AND DEVICES," (University of Dayton, Dayton, Ohio, 2017).
43. R. Ell, U. Morgner, F. X. Kärtner, J. G. Fujimoto, E. P. Ippen, V. Scheuer, G. Angelow, T. Tschudi, M. J. Lederer, A. Boiki, and B. Luther-Davies, "Generation of 5-fs pulses and octave-spanning spectra directly from a Ti:sapphire laser " Optics Letters **26**, 373-375 (2001).

44. J. Ma, Z. Qin, G. Xie, L. Qian, and D. Tang, "Review of mid-infrared mode-locked laser sources in the 2.0 μm–3.5 μm spectral region," Applied Physics Reviews **6**, 021317 (2019).
45. M. Durand, A. Houard, K. Lim, A. Durécu, O. Vasseur, and M. Richardson, "Study of filamentation threshold in zinc selenide," Optics Express **22**, 5852-5858 (2014).
46. A. Major, F. Yoshino, I. Nikolakakos, J. S. Aitchison, and P. W. E. Smith, "Dispersion of the nonlinear refractive index in sapphire," Optics Letters **29**, 602-604 (2004).
47. S. Yefet and A. Pe'er, "A Review of Cavity Design for Kerr Lens Mode-Locked Solid-State Lasers," Applied Sciences **3**, 694-724 (2013).
48. S. Vasilyev, M. Mirov, and V. Gapontsev, "Mid-IR Kerr-Lens Mode-Locked Polycrystalline Cr2+:ZnS Laser with 0.5 MW Peak Power," in *Advanced Solid State Lasers*, OSA Technical Digest (online) (Optical Society of America, 2015), AW4A.3.
49. D. T. F. Marple, "Refractive Index of ZnSe, ZnTe, and CdTe," Journal of Applied Physics **35**, 539-542 (1964).
50. E. Sorokin, "Solid-State Materials for Few-Cycle Pulse Generation and Amplification," in *Few-Cycle Laser Pulse Generation and Its Applications*, F. X. Kärtner, ed. (Springer-Verlag Berlin Heidelberg, Germany, 2004), pp. 3-73.
51. S. Vasilyev, I. Moskalev, M. Mirov, V. Smolski, S. Mirov, and V. Gapontsev, "Ultrafast middle-IR lasers and amplifiers based on polycrystalline Cr:ZnS and Cr:ZnSe " Optical Material Express **7**, 2636-2650 (2017).
52. S. Vasilyev, I. Moskalev, M. Mirov, S. Mirov, and V. Gapontsev, "Multi-Watt mid-IR femtosecond polycrystalline Cr^{2+}:ZnS and Cr^{2+}:ZnSe laser amplifiers with the spectrum spanning 2.0-2.6 um " Optics Express **24**, 1616-1623 (2016).
53. T. Popmintchev, M.-C. Chen, D. Popmintchev, P. Arpin, S. Brown, S. Ališauskas, G. Andriukaitis, T. Balčiunas, O. D. Mücke, A. Pugzlys, A. Baltuška, B. Shim, S. E. Schrauth, A. Gaeta, C. Hernández-García, L. Plaja, A. Becker, A. Jaron-Becker, M. M. Murnane, and H. C. Kapteyn, "Bright Coherent Ultrahigh Harmonics in the keV X-ray Regime from Mid-Infrared Femtosecond Lasers," Science **336**, 1287 (2012).

54. Yefet, S. & Pe'er, A. A review of cavity design for kerr lens mode-locked solid-state lasers. *Appl. Sci.* **3**, 694–724 (2013).

55. Magni, V., Cerullo, G. & De Silvestri, S. Closed form gaussian beam analysis of resonators containing a kerr medium for femtosecond lasers. *Opt. Commun.* **101**, 365–370 (1993).

56. Bouma, B. & Fujimoto, J. Compact kerr-lens mode-locked resonators. *Opt. lett.* **21**, 134–136 (1996).

57. Kimura, S., Tani, S. & Kobayashi, Y. Kerr-lens mode locking above a 20 ghz repetition rate. *Optica* **6**, 532–533 (2019).

58. Bouma, B., Ramaswamy-Paye, M. & Fujimoto, J. Compact resonator designs for modelocked solid-state lasers. *Appl. Phys. B: Lasers Opt.* **65**, 213–220 (1997).

59. Weiner, A. *Ultrafast Optics*, vol. 72 of *Wiley Series in Pure and Applied Optics* (Wiley, New York, NY, 2008), 1 edition

60. Lancaster, A. *Mid-ir waveguide lasers in transition metal doped ii-vi semiconductors*. Ph.D. thesis, Heriot-Watt University, Edinburgh (2017).